NSU
NOVA SOUTHEASTERN UNIVERSITY
NSU Libraries

Nova Southeastern University
NSUWorks

Theses and Dissertations

HCNSO Student Work

4-29-2016

Systematic Patterning of Sediments in French Polynesian Coral Reef Systems

Andrew Calhoun
ac6320@gmail.com

This document is a product of extensive research conducted at the Nova Southeastern University Halmos College of Natural Sciences and Oceanography. For more information on research and degree programs at the NSU Halmos College of Natural Sciences and Oceanography, please click here.

Follow this and additional works at: http://nsuworks.nova.edu/occ_stuetd

Part of the Geology Commons, Marine Biology Commons, and the Sedimentology Commons

Share Feedback About This Item

NSUWorks Citation

Andrew Calhoun. 2016. *Systematic Patterning of Sediments in French Polynesian Coral Reef Systems.* Master's thesis. Nova Southeastern University. Retrieved from NSUWorks, . (406)
http://nsuworks.nova.edu/occ_stuetd/406.

This Thesis is brought to you by the HCNSO Student Work at NSUWorks. It has been accepted for inclusion in Theses and Dissertations by an authorized administrator of NSUWorks. For more information, please contact nsuworks@nova.edu.

HALMOS COLLEGE OF NATURAL SCIENCES AND OCEANOGRAPHY

Systematic Patterning of Sediments in French Polynesian Coral Reef Systems

By

Andrew Calhoun

Submitted to the Faculty of
Halmos College of Natural Sciences and Oceanography
in partial fulfillment of the requirements for
the degree of Master of Science with a specialty in:

Marine Biology

Nova Southeastern University

April, 2016

Thesis of
Andrew Calhoun

Submitted in Partial Fulfillment of the Requirements for the Degree of

Masters of Science:

Marine Biology

Andrew Calhoun
Nova Southeastern University
Halmos College of Natural Sciences and Oceanography

April, 2016

Approved:

Thesis Committee

Major Professor :_____
Sam Purkis, Ph.D.

Committee Member :_____
Paul (Mitch) Harris, Ph.D.

Committee Member :_____
Bernhard Riegl, Ph.D.

Table of Contents

Acknowledgements

I would like to thank my principle advisor, Dr. Sam Purkis for his guidance and encouragement throughout this thesis project. I have learned many valuable skills while working with Dr. Purkis that will permeate into my professional career. Dr. Purkis has played an integral part in preparing me for and guiding me into my career path.

I would also like to thank Jeremy Kerr for taking the time to share his knowledge of statistical analysis with me. Jeremy was a remarkable mentor who helped me understand the statistical analysis used in my thesis and explained the computer code that ran the analysis.

Thank you to my committee members, Dr. Bernhard Riegl and Dr. Mitch Harris for their expert advice throughout this thesis project.

Thank you to the Living Oceans Foundation for providing the means to collect samples for this thesis project.

Abstract

Through a discipline termed “comparative sedimentology”, modern carbonate depositional environments have been used extensively as analogs to aid in the interpretation of equivalent fossil systems. Using field samples, GIS and remote sensing data for three isolated carbonate platforms in the Pacific, this thesis seeks to examine relationships between grain texture and grain type and their environment of deposition. The motivation is to highlight relationships that have the potential to better understand facies relations on carbonate platforms, and thereby reduce uncertainty and increase accuracy of subsurface exploration. The results of this study show that on Raivavae, Tubuai, and Bora Bora: French Polynesia grain texture and type of collected sediment samples could be used to predict water depth and relative distance lagoonward from the reef rim with ≥ 73% and ≥ 67% accuracy, respectively. The predictive relationships; however, were largely site specific. The exception being that the same relationship between water depth and the abundance of mud and coral could be used on both Raivavae (accuracy = 81%) and Tubuai (accuracy = 78%). Additionally, the abundance of coral and *Halimeda* in sediment samples were able to classify samples as belonging to either the platform margin or platform interior environments on Raivavae, Tubuai, and Bora Bora with 75%, 65%, and 65% accuracy, respectively. Overall, the results of this study suggest that the abundance of coral holds potential to be utilized as a proxy for distance from the reef rim on modern and ancient isolated carbonate platforms dating back to the Miocene geological epoch.

Key Words: Isolated carbonate platform, Pacific Ocean, Petrographic analysis, Geostatistical modeling

1. Introduction

Given the propensity of fossil reefs and their associated detritus to form excellent water aquifers and hydrocarbon reservoirs, considerable effort has been dedicated to understanding their anatomy, scales of accumulation and petrography. The concept of "comparative sedimentology", whereby facies (i.e. distinct rock or sediment bodies) patterns are compared within and between geologic periods, has received particular attention. In this vein the use of modern carbonate depositional environments as analogs to ancient ones has risen to the fore. Through examination of three modern isolated carbonate platforms in the Pacific, this thesis will develop and test a comparative sedimentologic approach that might be utilized to more accurately interpret modern platform facies relations and ancient subsurface carbonate stratigraphies.

The complexity of subsurface carbonate systems hinders detailed direct characterization of their three dimensional anatomy. Information on their internal properties is gathered from wells or outcrops. Most of these observations are along a vertical profile and do not provide information in the lateral, which is problematic for geostatistical modeling. While seismic data and horizontal wells mitigate this bias to some extent, the lateral dimension of a buried system often remains vastly undersampled. Modern analogs allow for examination of lateral trends in carbonate depositional systems, and remote sensing coupled with ground-truth information has been used extensively to this end (Purkis *et al.*, 2007; Kaczmarek *et al.*, 2010; Rankey & Reeder, 2010; Harris *et al.*, 2011; Purkis *et al.*, 2012a; Purkis *et al.*, 2012b; Madden *et al.*, 2013; Harris *et al.*, 2014b; Purkis *et al.*, 2014).

Marine shallow water carbonate depositional systems have long served as modern analogs to fossil systems. The internal precipitation of calcium carbonate has been a common-life strategy for marine organisms since the Proterozoic, as has their construction of carbonate platforms. As favored by modern colonial scleractinian corals, reef forming organisms have typically adopted a niche in shallow well-lit tropical marine waters where they are capable of building vast carbonate edifices, or platforms, that persist into the rock record (Purkis *et al.*, 2015a). Tucker and Wright (2009) report five broad categories of carbonate platforms: rimmed shelves, ramps, epeiric platforms,

drowned platforms, and isolated platforms. This study concentrates on isolated platforms (i.e. shallow water carbonate accumulations surrounded by deep water).

Isolated platforms are situated in the deep ocean. Consequently, their margins are typically subjected to strong prevailing winds, swells and storm patterns, with the exposure regime around the platform dictated by its orientation with regard to prevailing open ocean hydrodynamics. Isolated platforms have a high-energy windward margin, typically unsheltered and therefore subjected to long-period open ocean swells. Occasionally, windward margins can be somewhat sheltered from the influence of incident swell by neighboring platforms or antecedent topography (i.e. elevation and relief of the Pleistocene subsurface). Windward margins are typically characterized by reefs, rubble and coarse grained carbonate detritus (Hine *et al.*, 1981). Finer sediments, such as fine sands and muds, are swiftly winnowed and transported from the windward margin towards the lower-energy platform-interior where they accumulate (Tucker & Wright, 2009; Purkis & Harris, 2016). Depending on the influence of currents in the platform-interior, fines might accumulate in thick deposits, else migrate further to the leeward margin, and ultimately may be lost down the platform flanks to form periplatform sediment wedges (Hine *et al.*, 1981; Eberli, 1989; Wilber *et al.*, 1990; Rees *et al.*, 2005; Harris *et al.*, 2011; Purkis *et al.*, 2012b; Betzler *et al.*, 2014; Harris *et al.*, 2014b). In reality, of course, the distribution of sediment is highly variable between and within platforms because of their complex topography and architecture that depart radically from text-book conceptual models (e.g. Purkis et al. 2015). Accounting for and understanding this variation has driven research on isolated platforms throughout the world, including the Bahamas (Illing, 1954; Imbrie & Purdy, 1962; Harris, 1979, 1983; Reijmer *et al.*, 2012; Harris *et al.*, 2014b; Purkis & Harris, 2016), Caribbean Sea (Triffleman *et al.*, 1992; Gischler & Zingeler, 2002), and Indo-Pacific (Weber & Woodhead, 1972; Yamano *et al.*, 2002; Purkis *et al.*, 2005; Gischler, 2006; Riegl *et al.*, 2007).

The goals of recent studies have been to better understand the makeup and geometry of carbonate facies within and among these platforms, the constraining factors that influence these products, and how this knowledge can be applied to create and

understand a better geostatistical model (Harris & Vlaswinkel, 2008; Rankey *et al.*, 2009; Rankey & Reeder, 2010; Harris *et al.*, 2011; Rankey & Reeder, 2011; Rankey & Garza-Pérez, 2012; Wasserman & Rankey, 2014). Specifically, a study by Rankey *et al.* (2011) on two Pacific atolls, Aitutaki & Maupiti, quantitatively confirmed the qualitative understanding that sediment texture and type are, to some degree, correlated with water depth and distance from the platform margin. The authors reported a significant positive correlation between the abundance of mud and fine sand with increasing water depth and distance lagoonward from the platform margin, on both atolls. This same positive trend was noted for the abundance of non-skeletal grains, while a negative correlation was reported for the abundance of coral fragments. Similarly, Wasserman and Rankey (2014) found an inverse relationship between coral and coralline algae grains and increasing distance from the platform margin.

The results from the aforementioned studies are reminiscent of a classic study by Ginsburg (1956). In this study, the author illustrated how the relative abundances of five major faunal grain types (*Halimeda*, coralline algae, coral, *Foraminifera* (foram), and mollusk) showed consistent variation along transects spanning three reef sub-environments (fore reef, outer reef arc, and back reef) of the South Florida reef tract. Much like the findings of Rankey *et al.* (2011) and Wasserman and Rankey (2014), Ginsburg (1956) found that coral and coralline algae reached maximum abundance proximal to the outer reef arc and decreased in abundance towards the back reef. The opposite trend was observed for *Halimeda*. Since the fundamental work of Ginsburg (1956), current studies, including this study, continue to evaluate the prevalence of these trends on a global basis.

Another question that has been thoroughly studied and debated in comparative carbonate sedimentology is the degree to which shallow water marine carbonate facies be linked to water depth (Rankey, 2004; Bosence, 2008; Purkis *et al.*, 2012a; Harris *et al.*, 2014b; Purkis *et al.*, 2015b)? The answer of which could be used to reconstruct paleodepths and paloenvironments from the textural and faunal grain type composition of carbonate rocks (Schlager, 2007). Studying a 2 km^2 site around Tavernier Key, FL within a depth range of 0 – 3 m, Bosence (2008) showed that the facies: off-mound *Thalassia*,

Porites, and *Spongites* all exhibited maximum facies abundance at distinct depth zones. Conversely, for a 400 km^2 study site off Key Largo, FL within a depth range of 0 – 9 m, Rankey (2004) reported that the facies: rudstone, grainstone, wackestone, shelf margin reef, and patch reef were not partitioned by depth. Likewise, Harris *et al.* (2014b) showed that on the Great Bahama Bank (> 100,000 km^2) the facies: rudstone, high-energy-grainstone, grainstone, mud-poor-packstone, mud-rich-packstone, wackestone, mudstone, and land span considerable depth ranges from 0 – 16 m. Here wackestone was the most depth-constrained facies with a depth range of 0 – 6 m. In Saipan lagoon (65 km^2) within a depth range of 0 – 30 m, Purkis and Vlaswinkel (2012) showed mixed results where the facies: bioclastic packstone, branching framestone, mixed siliclastic skeletal grainstone, and wackestone were constrained by narrow depth ranges. Whereas the facies: massive framestone, boundstone skeletal grainstone, hardground, and siliclastic grainstone occupied much wider depth ranges. However, from a 6,000 km^2 study site in the Red Sea with a depth range of 0 – 40 m, Purkis *et al.* (2015) showed that none of the four observed facies (wackestone, grainstone, boundstone, rudstone) were constrained by water depth. The variable results from these examples highlights the need to continue to examine the relationship between water depth and facies texture and type on other carbonate platforms.

1.1 Objectives

The goal of this thesis are to evaluate how well grain texture (i.e. grain size and sorting) and faunal grain type of collected sediment samples can be used to estimate the position on three French Polynesian isolated platform tops: Raivavae, Tubuai, and Bora Bora. Position was recorded as three separate measures: water depth, relative distance lagoonward from the reef rim, and environment of deposition (platform margin or platform interior). The premise being that if sedimentologic properties of a stratigraphy vary systematically with the position on the platform top of a modern isolated carbonate platform, the same relationships might conceivably hold for fossil subsurface systems which are notoriously difficult to understand from sparse borings, wells and outcrops.

Raivavae was treated as a developmental site to formulate and test a suite of mathematical models on their efficacy to predict position on the platform top based on

grain texture and faunal grain type of collected sediment samples. These models were then deployed using collected data from Tubuai and published data from Bora Bora (Gischler, 2011) in order to blind-test their efficacy. The best predictive model was statistically selected and examined for potential utility for work in the subsurface. The undertaking of this study involved: 1) granularmetric and petrographic analysis of surface sediment samples previously collected from Raivavae and Tubuai, 2) investigation into lateral trends in grain texture and faunal grain type with the use of remote sensing and GIS and 3), high-level geostatistical modelling.

2. Regional Setting and Geomorphology of Raivavae, Tubuai, and Bora Bora

Raivavae, Tubuai, and Bora Bora are part of the French Polynesia archipelago (Fig. 1A). Five smaller archipelagos make up the larger French Polynesia archipelago: Gambier, Tuamotu, Marquesas, Society, and Austral. Raivavae and Tubuai are located within the southwestern extent of the Austral Islands archipelago, located between 23°18' - 23°54' S, and 149°34' – 147°34' W (Fig. 1A, B, and C). Bora Bora is located in the western part of the Society archipelago between 16°26' - 16°34' S, and 151°47' – 151°42' W (Fig. 1A, D). The French Polynesia archipelago is located within the southeastern trade wind belt and experiences prevailing winds from the east southeast; however, swell is predominantly from the south southwest (Wisuki, 2012b, 2012a).

All three platforms possess a central, remnant, volcanic island and are surrounded by annular reef rims which form near-continuous barriers around their lagoons (Fig. 1B, C, and D).Conspicuously, the most prominent passes in the rim of both Raivavae and Tubuai are through their northern margins. Raivavae has a secondary pass in the southern rim and Tubuai has two secondary passes in the southwestern margin. Bora Bora possess a singular pass located on the western margin of the platform. Both Raivavae and Tubuai have several sand-cays, locally known as motus, atop their eastern, windward margins, while Bora Bora possess motus along its eastern, windward margin, and northern margin. Lagoonward of the reef crest, a back reef apron (maximum dip extent: Raivavae ~1.64 km; Tubuai ~2.32 km and Bora Bora ~ 2.64 km) grades gently into a deep lagoon

(maximum depth: Raivavae and Tubuai ~ 20 m and Bora Bora ~ 40 m (Gischler, 2011)) as shown in Figures 2A, B, and 3.

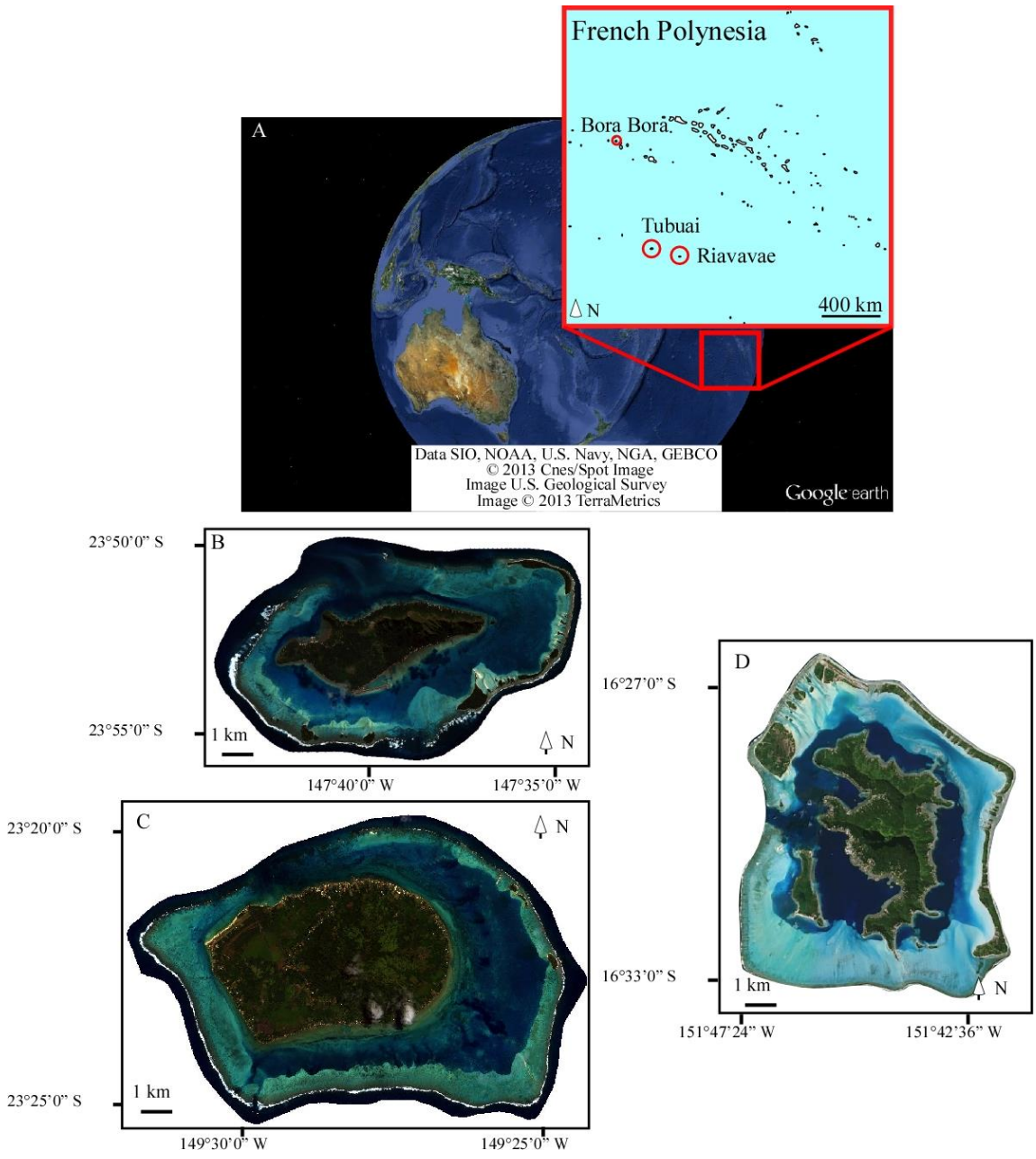

Figure 1: Location of French Polynesia in the central tropical Pacific Ocean (A). Inset shows the location of Raivavae, Tubuai, and Bora Bora in relation to the French Polynesian archipelago. WorldView-2 satellite imagery of Raivavae (B) and Tubuai (C), and SPOT satellite imagery of Bora Bora (ESRI) (D) show each platform to possess a fully aggraded reef margin surrounding a deep lagoon occupied by a remnant volcanic island.

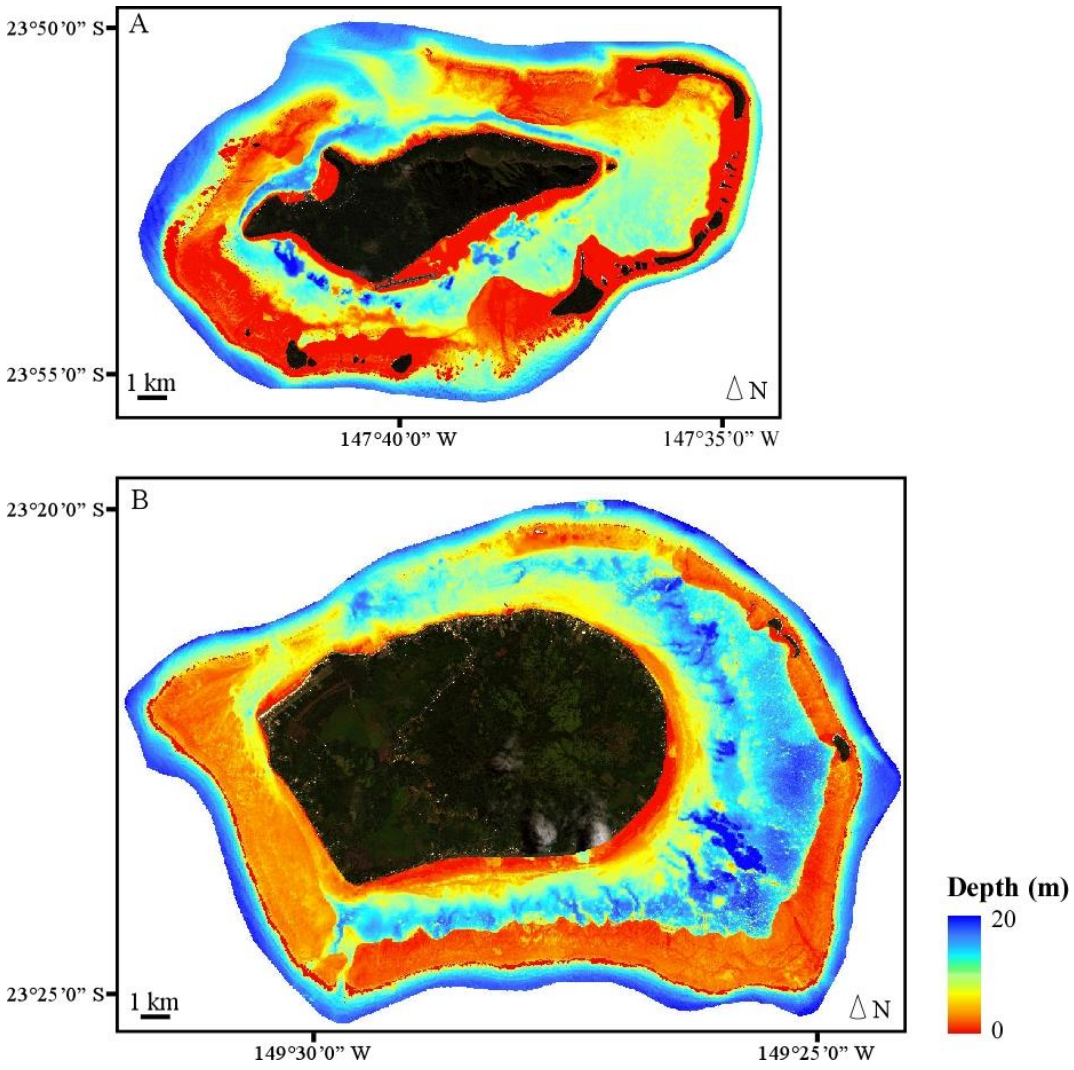

Figure 2: Bathymetric maps of Raivavae (A) and Tubuai (B) derived from spectral analysis of WorldView-2 satellite imagery calibrated by single-beam acoustic depth soundings acquired in the field.

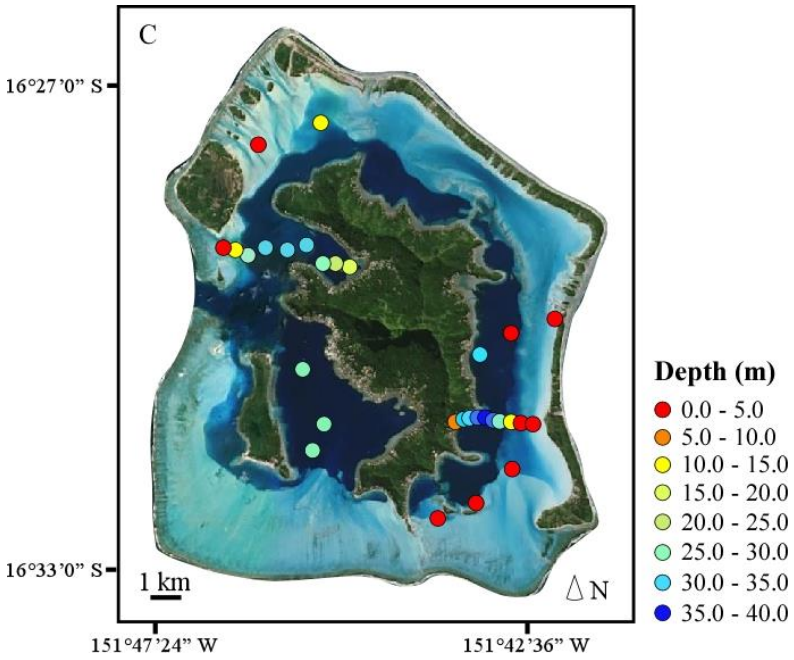

Figure 3: SPOT satellite imagery (ESRI) with overlain sediment sample locations that are color coded according to depth. Sample location and water depth obtained from Gischler (2011).

3. Methods

3.1 Sediment Sample Collection

Surficial sediment samples were collected from Raivavae (n = 28) and Tubuai (n = 21) as part of the Khaled Bin Sultan Living Oceans Foundation Global Reef Expedition in April 2013 (Fig. 4). Sediment samples were collected with a handcrafted sediment sampler (Fig. 5) made of a hollow metal cylinder with a fine meshed filter (< 0.03 mm) attached to the end. The sediment sampler was attached to a line, deployed from the deck of the boat, and dragged a few meters to ensure an adequate amount of sample was collected. As the sampler was pulled through the sediment, water flowed through the front opening of the sampler and out of the rear opening. Any sediment larger than 0.03 mm was retained in the sampler. Once aboard the boat, each sample was carefully transferred from the sampler to a 100 ml Nalgene bottle. GPS coordinates were recorded for each sample location. Water depth at the sample location was recorded using a single bean acoustic depth sounder (SyQwest, Inc.). At the end of each sampling day, the collected samples were decanted and dried in the main research vessel's laboratory oven

at 70°C for a 24 hour period. Fully dried samples were necessary for granularmetric and petrographic analysis of the sediment samples.

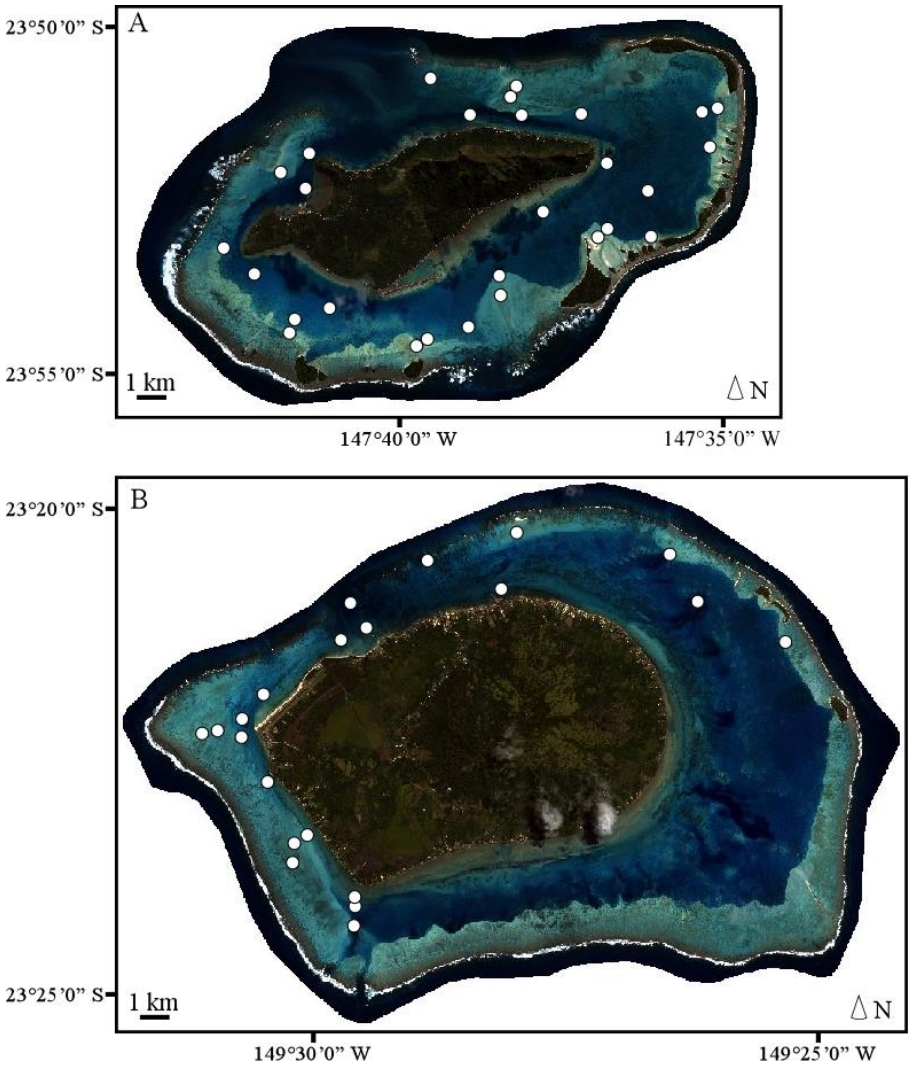

Figure 4: Worldview 2 satellite imagery of Raivavae (A), Tubuai (B) with overlain sample locations.

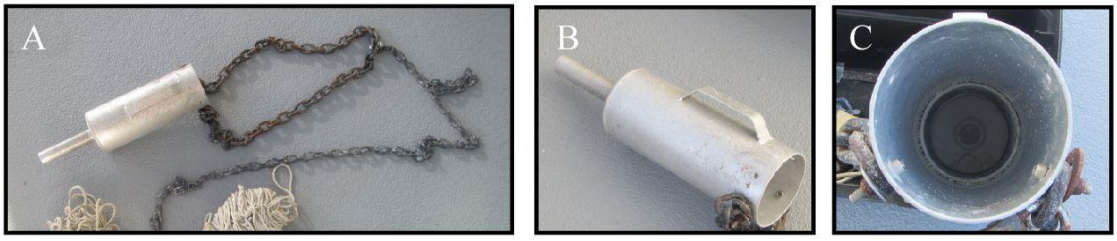

Figure 5: Photographs of the hand crafted sediment sampler (A and B) including an up-close view of the inside of the sampler showing the internal mesh filter (C).

3.2 Granularmetric Analysis of the Sediment Samples

Granularmetric analysis of the collected sediment samples was preformed to ascertain the grain size (*s*) distribution and sorting. For the purposes of this study, grain size distribution was described via percentages of gravel ($s > 2$mm), sand (0.062 mm $< s <$ 2mm), and mud ($s < 0.063$ mm). Each sample was weighed as a whole, emptied into a stack of two sieves with mesh sizes of 2 mm and 0.063 mm, respectively, and placed on a sieve shaker for five minutes to partition the sample into gravel, sand, and mud sized fractions. Each fraction was then weighed separately and calculated as a percentage of the whole sample. Next, sediment samples were analyzed for sorting using data measured by a CAMSIZER (Retsch Technology, Haan, Germany). The CAMSIZER is a particle size analyzer that utilizes a dual camera system to capture particle sizes ranging from 0.030 mm to 30 mm (Fig. 6). The CAMSIZER had limited capabilities to measure fine grains ($s < 0.063$ mm), so only the gravel and sand (coarse) size fractions were processed through the CAMSIZER. Data collected from the CAMSIZER were imported into GRADISTAT v8 (Blott & Pye, 2001) to calculate sorting (Folk & Ward, 1957) of the coarse size fraction of each sample (Table 1) .

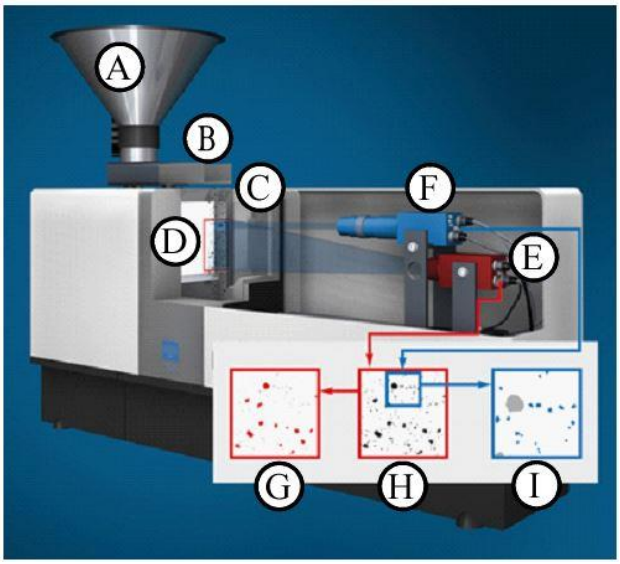

Figure 6: CAMSIZER by Retsch Technology. Sediment sample is poured into the sample funnel (A) that funnels the sediment onto the sample feeder (B). Vibrations from the sample feeder transport grains across the feeder and over the feeder's edge where they cascade into the measurement shaft (C). The illumination unit (D) lights up the measurement shaft, and allows real time recording of grains as they fall into the measurement shaft. The basic camera (E) captures grains 0.300 mm – 30 mm in diameter, while the zoom camera (F) captures grains 0.030 mm – 3 mm in diameter. Picture frames (G) and (I) illustrate measurements from the basic and zoom camera respectively, while picture frame (H) illustrates their combined measurements. (Image courtesy of http://www,retsch-technology.com).

Table 1: Sorting classifications and their corresponding phi values based on Folk & Ward (1957). Phi is the negative log of the diameter (mm) of a sediment grain.

Sorting Classification	**Range in Phi (φ)**
Very well sorted	0.00 - 0.35
Well sorted	0.35 - 0.50
Moderately well sorted	0.50 - 0.71
Moderately sorted	0.71 - 1.00
Poorly sorted	1.00 - 2.00
Very poorly sorted	2.00 - 4.00

3.3 Petrographic Analysis of the Sediment Samples

Petrographic analysis was preformed to ascertain the faunal grain type composition of each collected sediment sample. The sand fraction of each sample was separated from the gravel with a 2 mm sieve. Only the sand-size fraction was used for petrographic analysis due to the ubiquitously low abundance of gravel and mud. After separation, a sediment splitter split the sand fraction of each sample four times to obtain a 6.25 ml sub-sample of the original 100 ml sample (Fig. 7). Sub-samples containing greater than 50% sand sized grains less than 0.250 mm (very fine sand) were too fine to be analyzed under a binocular microscope. These samples (n = 15) were sent to National Petrographic Service, Inc. to be made into thin sections that could be examined and point-counted with a petrographic microscope. All other samples were point counted as loose grains under a binocular microscope.

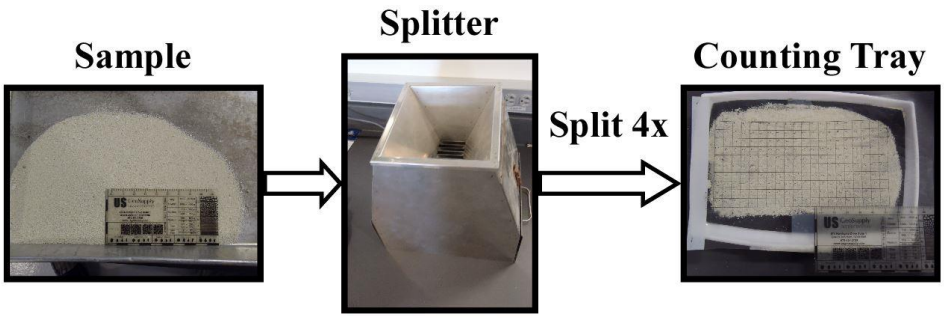

Figure 7: Illustration of the steps used to split a sample in preparation for point-counting loose sediment for faunal grain types. The sample is split four times to create a subsample that is 16 times smaller than the original sample (100 ml to 6.25 ml). The sample is then spread out uniformly on the counting tray to be examined under a binocular microscope.

Point-counting was used to calculate the faunal grain type composition of each sediment sample utilizing 11 biogenic categories: bryozoan, coral, coralline algae, mollusk, *Halimeda*, echinoderm, *Foraminifera* (foram), octocoral spicule (spicule), serpulid, crustacean and unknown (Appendix A). The thin section samples (n = 15) were photographed with a microscope slide scanner PathScan Enabler IV (Electron Microscopy Sciences, Hatfield, PA) to create a digital image of the slide (Fig. 8). These

images were imported into Coral Point Count with Excel extensions (CPCe) (Kohler & Gill, 2006) to create a uniform 400 point reference grid over each petrographic scan. A petrographic microscope was used to identify grain types in thin section. This was done by cross-referencing each point on the 400 point digital reference grid with the corresponding point on the thin section. This was repeated until 200 grains were identified. Blank spaces were skipped. The remaining samples (n = 34), were uniformly spread onto a small rectangular tray with a transparent 200 point grid overlain atop the sample (Fig. 7). A binocular microscope was used to visually identify grains at each grid point for each sample. The abundance of each faunal grain type was recorded as a relative percentage of the sample. Literature by Scholle and Ulmer-Scholle (2003) and Flügel (2004) were consulted when identifying grain types.

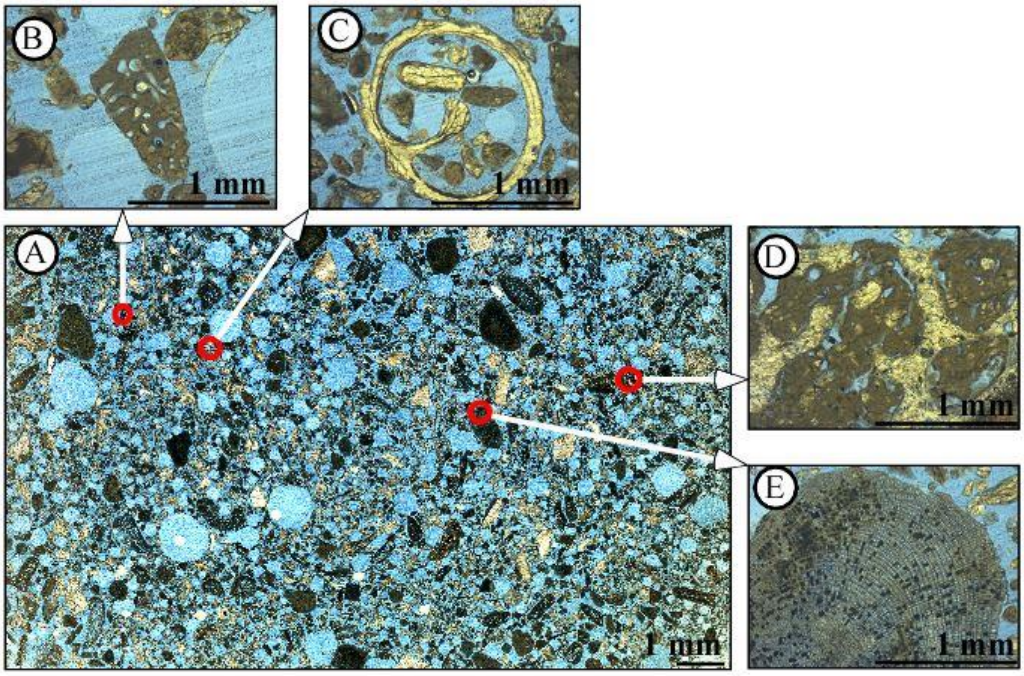

Figure 8: Photomicrograph of a thin section (sample FPA-16) taken by PathScan Enabler IV (A). Grains are black, grey, brown, and white. The blue background is the epoxy used to create the thin section. The large holes in the thin section are air bubbles that formed when the epoxy cured. The red circles highlight the location of examples (B) – (E). *Halimeda* fragment (B), characterized by reddish brown color and porous internal structure. Mollusk shell (C), characterized by large partitioned chambers. Coral fragment (D), characterized by a white skeleton and brown skeletal interstitial space filled with mud-sized sediments. Coralline algae fragment (E), characterized by reddish brown color and concentric cells that radiate from the center of the grain.

3.4 Delineating the Platform Margin and Platform Interior from Satellite Imagery

Satellite imagery was interpreted to manually delineate the platform margin (margin), the platform interior (interior), and the central island of Raivavae, Tubuai, and Bora Bora using ArcMap10.3 (ESRI). Sediment samples were assigned to either the margin or interior based on these delineations. For the purpose of this thesis, the margin was defined as the zone extending from the reef rim to the lagoonal termination of the back reef sand apron (LTBRA) (Fig. 9B, C). The reef rim was defined from the satellite

imagery as the transition from the dark brown reef flat and the open ocean, and characterized by breaking waves (Fig. 9A, B). The LTBRA was defined as the sharp color change between the light-blue back reef apron and dark-blue lagoon (Fig. 9A, B). The interior was delineated as the lagoon, spanning from the LTBRA to the central island (Fig. 9B, C). The central island was delineated by the perimeter of its shoreline (Fig. 9B).

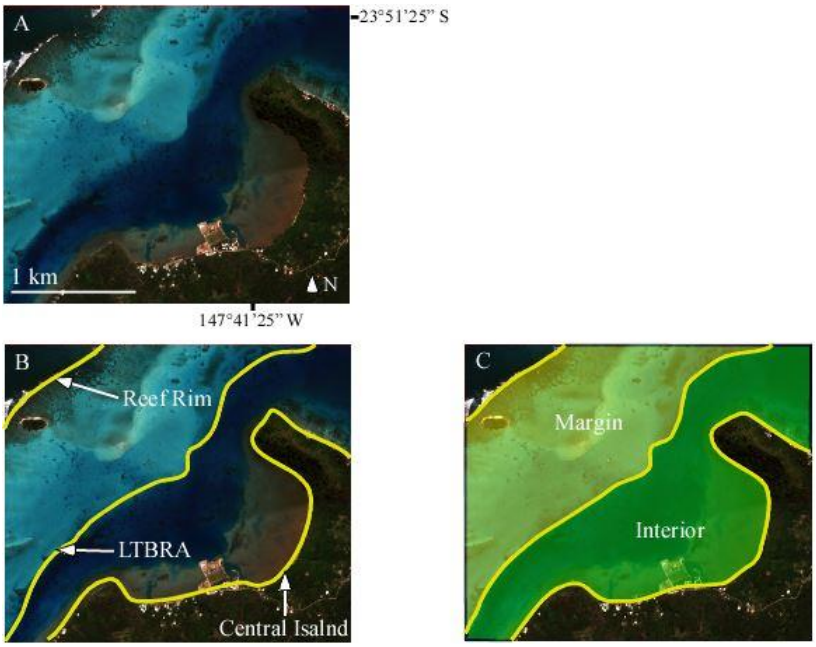

Figure 9: WorldView-2 image subscenes of Raivavae showing an example of the imagery used to delineate the reef rim, LTBRA, and the central island (A); delineations (yellow) of the reef rim, the LTBRA, and the central island (B); and extents of the margin and interior as confined by these delineations (C).

3.5 Calculating Relative Distance of a Sediment Sample from the Reef Rim

Relative distance was used as a measure to quantify the distance of a sediment sample from the reef rim. Using relative distance allowed for easier comparison of distance between the three different sized platforms. First, to calculate relative distance from the reef rim (RDRR), the shortest straight line distance from the delineation of the reef rim to a sediment sample location was measured as a transect in GIS (Fig. 10A). Second, the transect was extended past the sediment sample location to the delineation of

the central island to measure the total length of the transect (Fig. 10B). Finally, these two measurements were used in the following equation to calculate RDRR (Fig. 10C):

$$RDRR = \frac{D_1}{D_2} \quad (1)$$

where D_1 is the distance measured from the delineation of the reef rim to a sediment sample location, and D_2 is the total distance of the respective transect spanning from the reef rim to the central island.

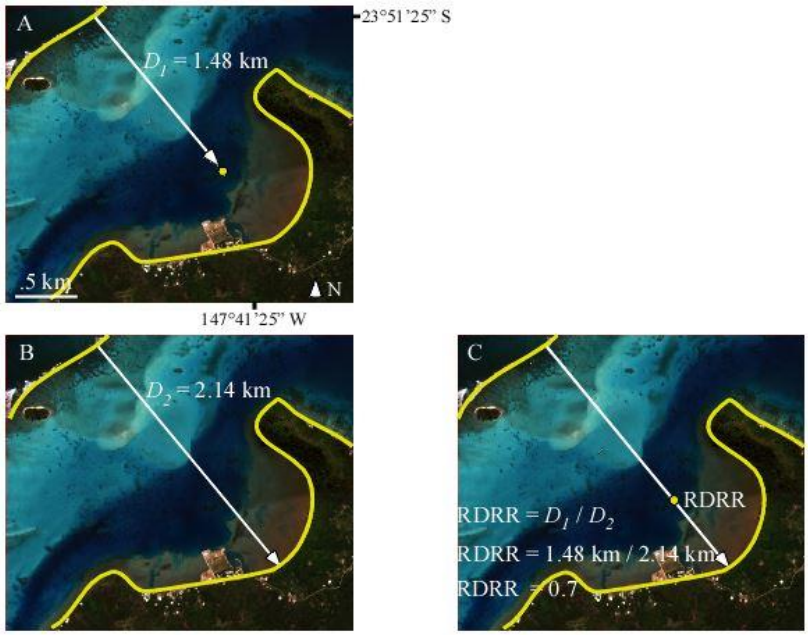

Figure 10: WorldView-2 Image subscenes of Raivavae demonstrating the process of measuring the distance from the reef rim to a sediment sample location, D_1, (A), measuring the distance of the transect spanning from the reef rim to central island, D_2, (B) and calculating RDRR from D_1 and D_2 (C). The white lines are transects with arrows indicating the direction in which each transect spans. The yellow circles represent sediment sample locations.

4 Statistical Methods

4.1 Formulating Models to Predict Water Depth and RDRR

A set of 22 statistical models were formulated to test how well the response variables, water depth and RDRR, could be predicted based on sediment character. Six

sedimentary properties were used as explanatory variables: percent gravel, percent sand, percent mud, sorting, percent coral, and percent *Halimeda*. Of the eleven faunal grain type categories, only coral and *Halimeda* were used in the statistical modeling because they were present in all sediment samples, and these fauna can be associated with particular environments of deposition. In particular, coral is prevalent in marginal, reef rim environments while *Halimeda* has been reported as a common constituent within interior, lagoonal environments (Hillis-Colinvaux, 1980; Braga *et al.*, 1996; Chevillon, 1996; Yamano *et al.*, 2002; Montaggioni, 2005; Tucker & Wright, 2009; Rankey *et al.*, 2011; Wasserman & Rankey, 2014). However, *Halimed*a has also been reported to be a major constituent in marginal settings of some reef systems. Consequently, the abundance of *Halimeda* within the margin and interior varies between reef systems (Gischler, 2011).

For each of the two response variables, the set of 22 statistical models included six linear models, 15 multilinear models, and one random model. The set of models was limited to two sedimentary properties because the low sample size of the study sites (Raivavae: n = 28, Tubuai: n = 21, and Bora Bora: n = 31) would result in statistically unreliable models for three or more explanatory variables (Babyak, 2004). The linear models took the form of:

$$y = \beta_0 + \beta_1 x_1 \tag{2}$$

where y is the response variable (water depth or RDRR), x_1 is the explanatory variable (one of the six sedimentary properties), and the variables β_0 and β_1 are statistical coefficients fitted through linear regression. The multilinear models are similarly structured such that two explanatory variables are paired. They take the form of:

$$y = \beta_0 + \beta_1 x_1 + \beta_2 x_2 \tag{3}$$

where x_2 is a second explanatory variable and β_2 is a statistical coefficient fitted through multilinear regression. Finally, the random model takes the form:

$$y = \beta_0 \tag{4}$$

such that the response variable y is not related to an explanatory variable.

The two sets of 22 models were used for the Raivavae and Tubuai datasets. For Bora Bora, two sets of only four models were used, because percent coral and percent *Halimeda* were the only two sedimentary properties from the Gischler (2011) dataset that were readily comparable to the Raivavae and Tubuai datasets. Three linear models: percent coral, percent *Halimeda*, and random, and one multi-linear model: percent coral and percent *Halimeda* were used for Bora Bora.

4.2 Applying Models to the Study Sites

The two sets of models were applied to each study site dataset. First, each dataset was partitioned into three subgroups: platform-wide (i.e. all samples), margin (i.e. margin samples), and interior (i.e. interior samples). This allowed the models to be assessed on their ability to predict water depth and RDRR for the entire platform, the margin, and the interior separately. The lm() function (i.e. regression analysis) in R 3.0 was used to estimate a line of best fit for each model as applied to each dataset subgroup (Team, 2014). The line of best fit was estimated based on the set of explanatory and observed response variables for each dataset subgroup. The statistical coefficients and a new set of predicted response variables for each model were estimated from the line of best fit.

4.3 Assessing the Accuracy of the Predictive Models

The accuracy of each model was evaluated by calculating the root mean squared error (RMSE). The RMSE gives a mean value of the error, or difference, between the predicted and observed response variables (Burnham & Anderson, 2002). Low RMSE values indicate little difference between the predicted and observed variables, and thus indicate a more accurate model. RMSE was calculated with the following equation:

$$\mathrm{RMSE} = \sqrt{\frac{\sum_{i=1}^{n} (\hat{y}_i - y_i)^2}{n}} \tag{5}$$

where $\hat{y}_i$ is the set of predicted response variables, y_i is the set of observed response variables, and n is the sample size. RMSE for models predicting RDRR was on a scale of 0 – 1 (0% - 100% of total transect length), while RMSE for models predicting water depth was in meters. The RMSE of each model was then normalized (NRMSE) to the range of water depth or RDRR measurements within the respective subgroup.

Normalizing the RMSE provided a context for the accuracy of each model given these ranges. NRMSE was on a scale of 0 – 1, and gives the overall error of the model.

$$\text{NRMSE} = \frac{\text{RMSE}}{y_{\max} - y_{\min}} \quad (6)$$

Based on NRMSE, each set of models for each dataset subgroup of Raivavae and Tubuai were narrowed down to the five most accurate models. Out of these five models, the model that showed the greatest accuracy across all three subgroups was selected as the most applicable model for the study site. Bora Bora only had four models to choose from, so the one model out of the four that showed the greatest accuracy across all three subgroups was selected.

4.4 Applying Raivavae Models to Tubuai and Bora Bora

Raivavae models were also tested on Tubuai and Bora Bora to examine their aptitude to predict water depth and RDRR on other, similar, isolated carbonate platforms. The one-water depth and RDRR model selected from the top five Raivavae models were tested on Tubuai. For Bora Bora, the most accurate Raivavae water depth and RDRR model out of the set of four applicable models: percent coral, percent *Halimeda*, random, and percent coral and percent *Halimeda* was applied. The model coefficients from the Raivavae models were kept, while the explanatory variables from Tubuai and Bora Bora were used. Running the models with Raivavae coefficients and Tubuai and Bora Bora explanatory variables allowed for a new set of response variables to be estimated for each site. RMSE was applied using the new set of response variables, and NRMSE calculated from RMSE. The accuracy of the Raivavae models as applied to Tubuai and Bora Bora would thus reveal if statistical trends observed from Raivavae were also apparent for Tubuai and Bora Bora.

4.5 Linear Discriminant Analysis

Linear discriminant analysis (LDA) was used to test how accurately a sedimentary property or combination of sedimentary properties could differentiate between the margin and interior environments. LDA is a statistical means of using a linear combination of variables to separate two or more classes of data (Fisher, 1936).

This metric is similar to the ANOVA test in that it attempts to define a response variable based on a linear combination of explanatory variables (Fisher, 1936; McLachlan, 2004). However, LDA differs from ANOVA in that it uses continuous data (e.g. percent sand) as the explanatory variables and categorical data (e.g. margin or interior) as the response variables; whereas the methodology of ANOVA is the opposite (Wetcher-Hendricks, 2011). First, box and whisker plots of the abundance of each sedimentary property by each subgroup were analyzed to gauge which of the six candidate sedimentary properties would likely show differentiation by the margin and interior. Any sedimentary properties that showed no overlap of the lower and of the upper quartiles (i.e. upper and lower whiskers) when comparing between margin and interior were chosen to be used as a variable in LDA because they had the least overlap of data and would most likely produce the best differentiation between the margin and interior. The selected sedimentary properties were then subjected to LDA to formulate a model to differentiate between the margin and interior.

Leave one out cross validation (LOOCV) was used to test the accuracy of the formulated LDA model. LOOCV works by removing one entry from the dataset and training the model to best predict the removed entry (Lachenbruch & Mickey, 1968). This procedure is repeated for each entry in the dataset to estimate the overall accuracy of the model. This methodology was used to formulate a LDA model for each of three datasets. The LDA model from each dataset was additionally tested on the other two datasets to evaluate if a singular LDA model could be used among platforms.

5. Results

5.1 Sedimentary Properties

5.1.1 Raivavae and Tubuai

The textural character of Raivavae and Tubuai sediments were similar in many ways; however, there were clear differences that separate sediments from these two platforms. Raivavae and Tubuai can be characterized by a prominence of sand sized grains, both in the margin and interior. Gravel was far less abundant, while mud was scarce, on both (Fig. 11A, B and Appendix B, Tables 1 and 3). On Raivavae, sand decreased in abundance from the margin (mean = 85.59%) to the interior (mean =

79.86%), while the abundance of sand remained consistent from the margin (mean = 76.07%) to the interior (mean = 78.33%) of Tubuai. The decrease in sand in the interior of Raivavae was balanced by an increase in mud (mean: margin = 0.36% and interior = 7.34%). Gravel remained virtually constant between the margin (mean = 14.14%) and interior (mean = 12.71%) of Raivavae. In contrast, gravel decreased in abundance from the margin (mean = 23.53%) to the interior (12.00%) of Tubuai. This decrease was balanced with an increase in mud in Tubuai's interior (mean: margin = 0.40% and interior = 9.67%). The increase in the abundance of mud in the interior of Tubuai was primarily influenced by high concentrations of mud measured from sediment samples FPA-57 (mud = 18.00%) and FPA-70 (mud = 35.00%). Sorting of Raivavae sediments range from poorly sorted to very poorly sorted, with margin and interior sediments averaging as very poorly sorted (Fig. 12A and Appendix B, Table 1). Sorting of Tubuai sediments ranged from moderately sorted to poorly sorted, with margin and interior sediments averaging as poorly sorted (Fig. 12B and Appendix B, Table 3).

Faunal grain types observed in Raivavae and Tubuai sediments were very similar as well; however, there were also clear differences that distinguished these two sites (Fig. 13A and B and Appendix B, Tables 2 and 4). The main faunal grain types observed from both sites were: coral (mean: Raivavae = 27.21% and Tubuai = 23.55%), coralline algae (mean: Raivavae = 9.96% and Tubuai = 11.35%), *Halimeda* (mean: Raivavae = 33.61% and Tubuai = 27.20%), and mollusk (mean: Raivavae = 19.43% and Tubuai = 26.05%). For both sites the abundance of coral and mollusks were the greatest in the margin. On Raivavae, coral showed a marked decrease in abundance from the margin (mean = 34.57%) to the interior (mean = 19.86%), while mollusks showed a lesser decrease (mean: margin = 21.57% and interior = 17.29%). On Tubuai, the decrease in coral from the margin to the interior was not a drastic (margin mean = 24.60% and interior mean = 20.83%). The same was true for the abundance of mollusks (mean: margin = 27.00% and interior = 23.33%). Coralline algae showed a greater abundance in Raivavae's margin (mean = 11.07%) than the interior (mean = 8.86%). In contrast, coralline algae displayed a slight increase in abundance from the margin (11.07%) to the interior (12.33%) of Tubuai. For both sites, *Halimeda* was greatest in the interior (mean: Raivavae = 43.79% and Tubuai = 33.00%) with a decrease in the margin (mean: Raivavae = 23.43% and

Tubuai = 24.80%). The other faunal grain types (bryozoan, echinoderm, foram, spicule, serpulid, and crustacean) observed in Raivavae and Tubuai sediment samples did not exceed a mean of more than 2.36% and 3.87%, respectively. Unknown grains had a mean of 6.50% and 7.15% for Raivavae and Tubuai, respectively.

5.1.2 Bora Bora

The only sedimentary data obtained for Bora Bora was the abundance of coral and *Halimeda*. These data, along with water depth recordings for the Bora Bora sediment samples, were obtained from Gischler (2011). Appendix B, Table 5 contains this data along with measurements of RDRR for each Bora Bora sediment sample.

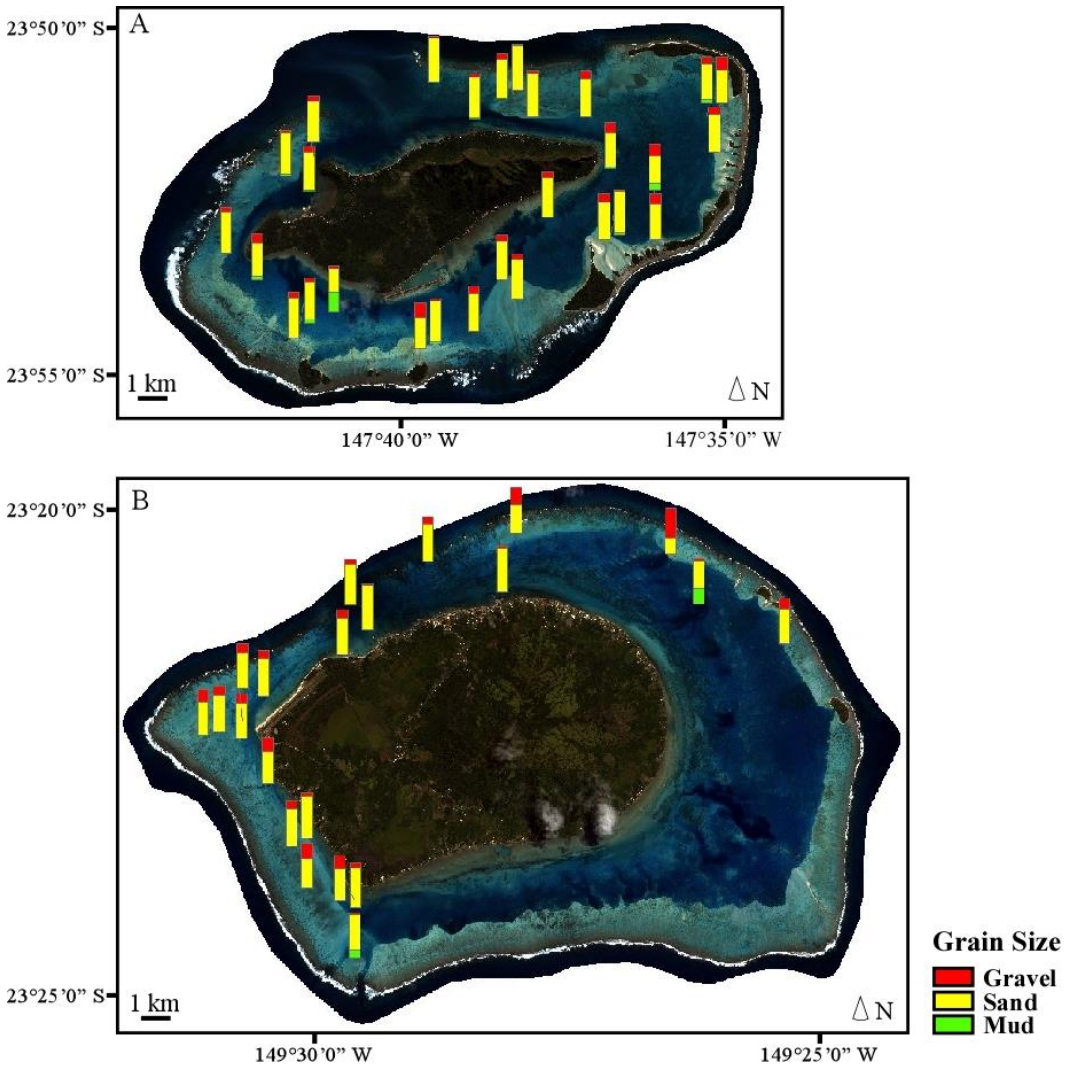

Figure 11: WorldView-2 satellite imagery of Raivavae (B) and Tubuai (B) with overlain bar charts that represent the abundance of gravel (red), sand (yellow) and mud (green) of every collected sediment sample.

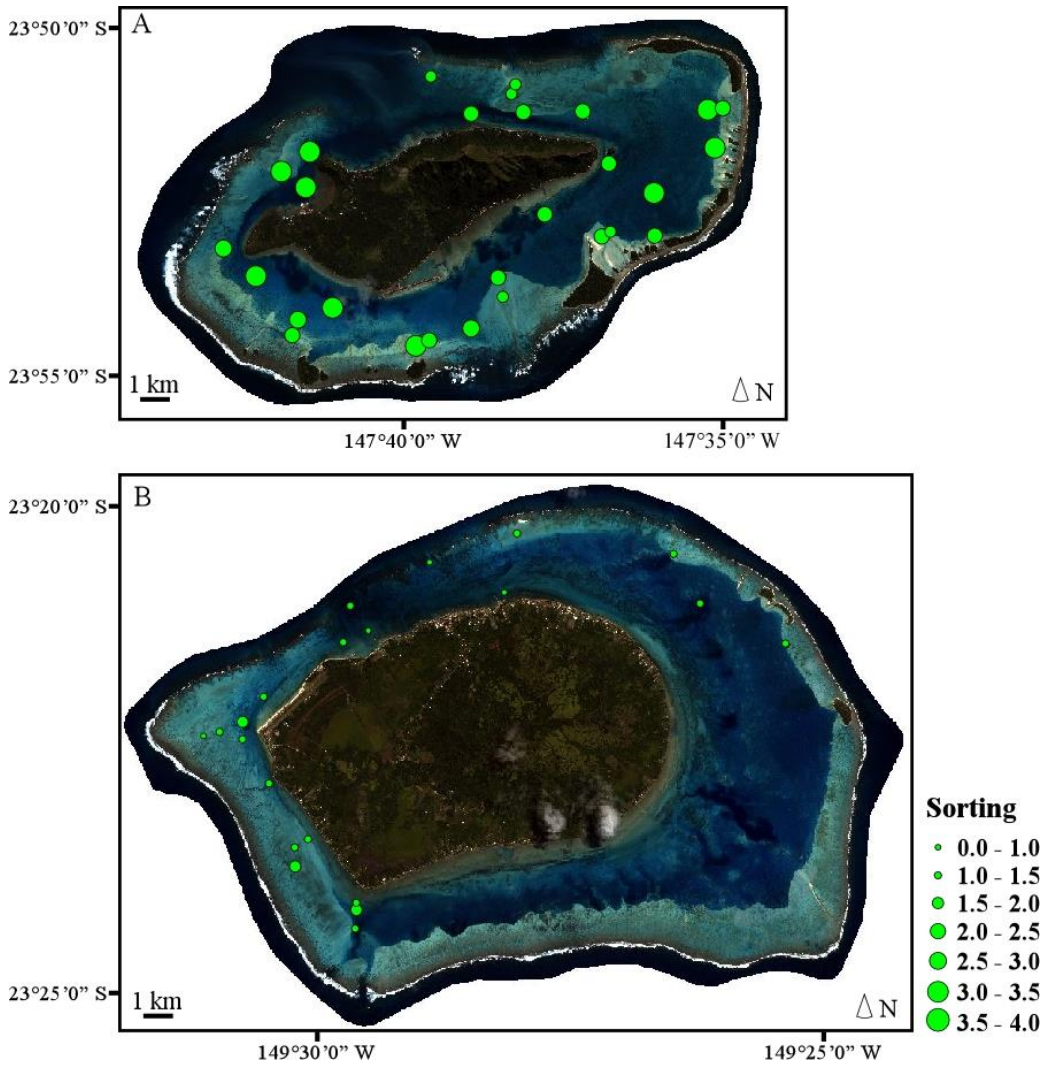

Figure 12: WorldView-2 satellite imagery of Raivavae (A) and Tubuai (B) with overlain circles that represent the sorting of every collected sediment sample.

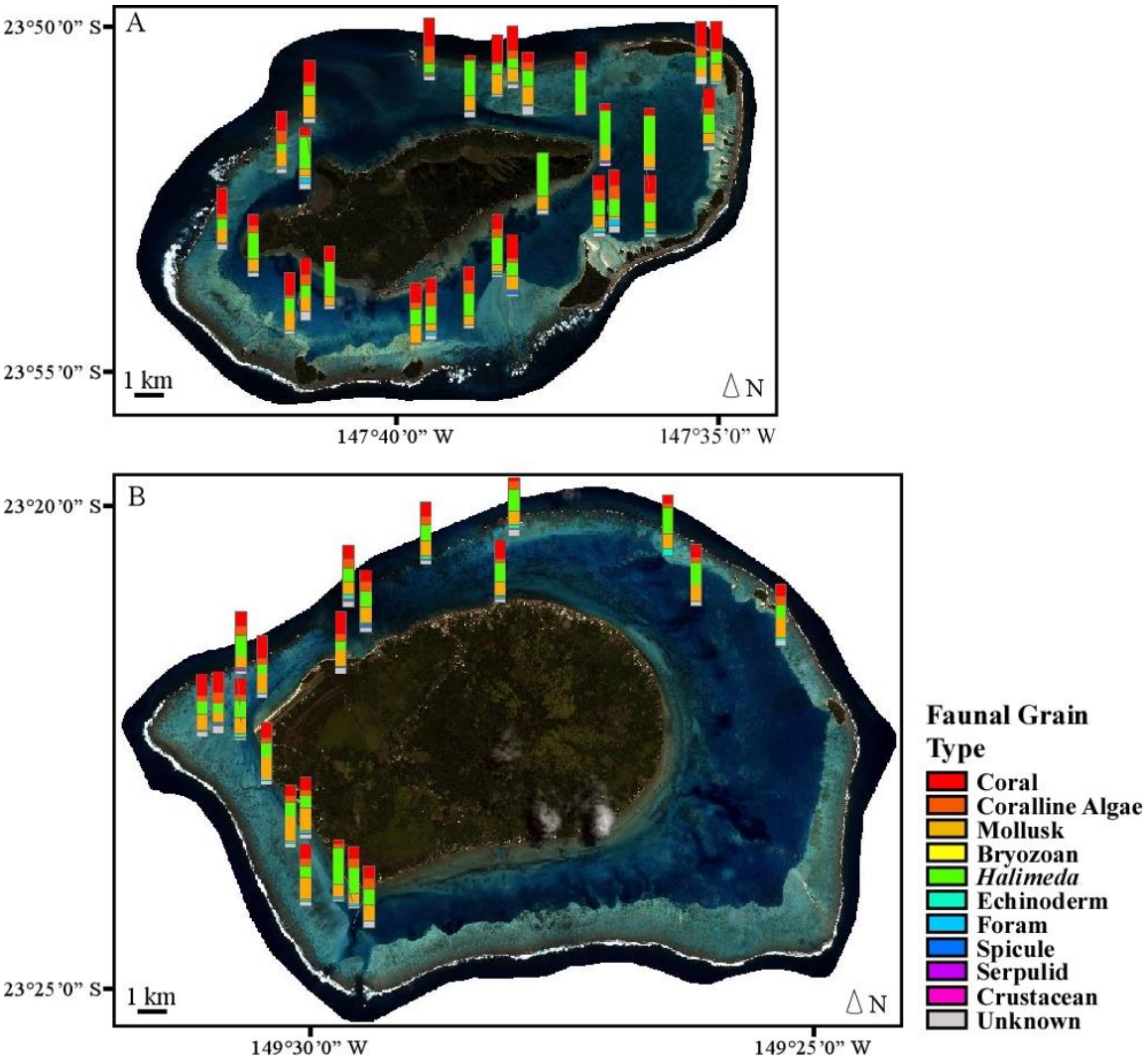

Figure 13: WorldView-2 satellite imagery of Raivavae (A) and Tubuai (B) with overlain bar charts that represent the faunal grain type composition of every collected sediment sample.

5.2 Sedimentary Properties Showed Mixed Performance for Predicting Water Depth

5.2.1 Raivavae and Tubuai Models

Overall, the selected sedimentary properties showed the greatest applicability to predict water depth within the platform-wide and margin subgroups of Raivavae and the platform-wide and interior subgroups of Tubuai (Appendix B, Tables 6 and 7). The model that could be applied most accurately to all three subgroups of the Raivavae

dataset predicted water depth based on percent mud and percent coral (NRMSE: platform-wide = 0.19, margin = 0.19, and interior = 0.23), as seen in Table 2. Applying this model to the Tubuai dataset resulted less accurate predictions (NRMSE: platform-wide = 0.22, margin = 0.31, and interior = 0.37). Conversely, the Tubuai model performed with greater accuracy (NRMSE: platform-wide = 0.11, margin = 0.21, and interior = 0.07), as seen in Table 3. This model predicted water depth based on percent gravel and percent mud.

Table 2: Summary of the top selected Raivavae water depth model as applied to the platform-wide, margin, and interior subgroups of the Raivavae and Tubuai datasets. Coefficients of the model vary by subgroup. RMSE of the model is given in meters. Depth range is also in meters, and represents the depth range of sediment samples used in the model. NRMSE (in bold) gives the error (on a scale of 0 – 1) of the model for the given depth range.

Top Selected Raivavae Water Depth Model as Applied to Raivavae and Tubuai				
Subgroup		**Platform-wide**	**Margin**	**Interior**
Model		DEPTH = 8.130 + 9.779MU – 15.243CR	DEPTH = - 0.022 + 16.079MU + 5.093CR	DEPTH = 0.563 + 0.735MU – 0.012CR
As Applied to Raivavae	**RMSE (m)**	2.69	0.69	2.65
	Depth Range (m)	0.72 - 14.88	0.72 - 2.56	3.52 - 14.88
	NRMSE	**0.19**	**0.19**	**0.23**
As Applied to Tubuai	**RMSE (m)**	4.79	3.53	7.47
	Depth Range (m)	0.74 - 21.76	0.74 - 12.11	1.64 - 21.76
	NRMSE	**0.22**	**0.31**	**0.37**
Note. The abbreviations MU and CR represent percent mud and percent coral, respectively				

Table 3: Summary of the top selected Tubuai water depth model as applied to the platform-wide, margin, and interior subgroups of the Tubuai dataset. Coefficients of the model vary by subgroup. RMSE of the model is given in meters. Depth range is also in meters, and represents the depth range of sediment samples used in the model. NRMSE (in bold) gives the error (on a scale of 0 – 1) of the model for the given depth range.

Top Selected Tubuai Water Depth Model as Applied to Tubuai			
Subgroup	**Platform-wide**	**Margin**	**Interior**
Model	Depth = 6.033 - 11.280GR + 48.765MU	Depth = 5.984 – 10.461GR – 195.764MU	Depth = 7.034 – 17.485GR + 46.613MU
RMSE (m)	2.27	2.43	1.48
Depth Range (m)	0.74 - 21.76	0.74 - 12.11	1.64 - 21.76
NRMSE	**0.11**	**0.21**	**0.07**
Note. The abbreviations GR and MU represent percent gravel and percent mud, respectively			

5.2.2 Raivavae and Bora Bora Models

Overall, coral and *Halimeda* were not accurate predictors of water depth for the Bora Bora dataset (Appendix B, Table 8). The most accurate model formulated from the Raivavae dataset suitable to be tested on the Bora Bora dataset predicted water depth based on percent coral and percent *Halimeda* (Table 4). This model showed variable accuracy as applied to the Raivavae subgroups (NRMSE: platform-wide = 0.19, margin = 0.38, and interior = 0.23). The Raivavae model showed a decrease in performance as applied to Bora Bora (NRMS: platform-wide = 0.44, margin = 0.31, and interior = 0.58). Comparatively, the Bora Bora model produced more accurate predictions of water depth (NRMSE: platform-wide = 0.25, margin = 0.27, and interior = 0.18), as seen in Table 5. This model also predicted water depth based on percent coral and percent *Halimeda*, but had different coefficients than the Raivavae model.

Table 4: Summary of the top selected Raivavae water depth model suitable to be applied to the Raivavae and Bora Bora datasets. The model was applied to the platform-wide, margin, and interior subgroups of each dataset. Coefficients of the model vary by subgroup. RMSE of the model is given in meters. Depth range is also in meters, and represents the depth range of sediment samples used in the model. NRMSE (in bold) gives the error (on a scale of 0 – 1) of the model for the given depth range.

Top Selected Raivavae Water Depth Model Suitable to be Applied to Raivavae and Bora Bora				
Subgroup		**Platform-wide**	**Margin**	**Interior**
Model		Depth = 6.629 - 12.415CR + 3.278HA	Depth = 1.146 + 3.398CR - 2.387HA	Depth = 10.890 - 14.725CR - 2.337HA
As Applied to Raivavae	**RMSE (m)**	2.72	0.7	2.68
	Depth Range (m)	0.72 - 14.88	0.72 - 2.56	3.52 - 14.88
	NRMSE	**0.19**	**0.38**	**0.24**
As Applied to Bora Bora	**RMSE (m)**	16.41	7.85	16.35
	Depth Range (m)	0 - 37	0 - 25	0 - 37
	RRMSE	**0.44**	**0.31**	**0.58**
Note. The abbreviations CR and HA represent percent coral and percent *Halimeda*, respectively				

Table 5: Summary of the top selected Bora Bora water depth model as applied to the platform-wide, margin, and interior subgroups of the Bora Bora dataset. Coefficients of the model vary by subgroup. RMSE of the model is given in meters. Depth range is also in meters, and represents the depth range of sediment samples used in the model. NRMSE (in bold) gives the error (on a scale of 0 – 1) of the model for the given depth range.

Top Selected Bora Bora Water Depth Model as Applied to Bora Bora			
Subgroup	**Platform-wide**	**Margin**	**Interior**
Model	Depth = 25.187 - 31.596CR - 28.822HA	Depth = 6.793 - 4.257CR - 3.912HA	Depth = 28.026 - 34.680CR + 3.535HA
RMSE (m)	9.14	6.86	4.92
Depth Range (m)	0 - 37	0 - 25	0 - 37
NRMSE	**0.25**	**0.27**	**0.18**
Note. The abbreviations CR and HA represent percent coral and percent *Halimeda*, respectively			

5.3 Sedimentary Properties Show Moderate Accuracy for Predicting Relative Distance from the Reef Rim

5.3.1 Raivavae and Tubuai Models

The selected sedimentary properties showed an overall decreased performance for predicting RDRR than for water depth for Raivavae and Tubuai (Appendix, Tables 9 and 10). Also, much like the water depth models, the most accurate predictions came from site-specific models. The model that could be applied most accurately to all three subgroups of the Raivavae dataset predicted RDRR based on percent sand and percent coral (Table 6). This model showed moderate accuracy for all three subgroups (NRMSE: platform-wide: 0.23, margin = 0.27, and interior = 0.24). The Raivavae model performed less accurately on Tubuai (NRMSE: platform-wide = 0.35, margin = 0.42, and interior = 0.39). Compared to the Raivavae model, the Tubuai model showed an increased accuracy (NRMSE: platform-wide = 0.32, margin = 0.33, and interior = 0.20), as seen in Table 7. This model predicted RDRR based on percent gravel and sorting.

Table 6: Summary of the top selected Raivavae RDRR model as applied to the platform-wide, margin, and interior subgroups of the Raivavae and Tubuai datasets. Coefficients of the model vary by subgroup. RMSE of the model is on a scale of 0 – 1, and represents 0% – 100% of total transect length spanning from the reef rim to the central island. NRMSE (in bold) gives the error (on a scale of 0 – 1) of the model for the range of RDRR measurements.

Top Selected Raivavae RDRR Model as Applied to Raivavae and Tubuai				
Subgroup		**Platform-wide**	**Margin**	**Interior**
Model		RDRR = 0.460 + 0.397SA – 0.993CR	RDRR = - 0.480 + 1.263SA - 0.468CR	RDRR = 0.900 – 0.098SA – 1.171CR
As Applied to Raivavae	**RMSE**	0.17	0.15	0.15
	Range of RDRR Measurements	0.17 – 0.89	0.17 – 0.72	0.27 – 0.89
	NRMSE	**0.23**	**0.27**	**0.24**
As Applied to Tubuai	**RMSE**	0.27	0.33	0.13
	Range of RDRR Measurements	0.09 – 0.86	0.09 – 0.86	0.45 – 0.81
	NRMSE	**0.35**	**0.43**	**0.39**
Note. The abbreviations SA and CR represent percent sand and percent coral, respectively				

Table 7: Summary of the top selected Tubuai RDRR model as applied to the platform-wide, margin, and interior subgroups of the Tubuai dataset. Coefficients of the model vary by subgroup. RMSE of the model is on a scale of 0 – 1, and represents 0% – 100% of total transect length spanning from the reef rim to the central island. NRMSE (in bold) gives the error (on a scale of 0 – 1) of the model for the range of RDRR measurements.

Top Selected Tubuai RDRR Model as Applied to Tubuai			
Subgroup	**Platform-wide**	**Margin**	**Interior**
Model	RDRR = 0.163 – 0.373GR + 0.352SO	RDRR = 0.131 – 0.334GR + 0.353SO	RDRR = 0.562 – 0.735GR + 0.012SO
RMSE	0.25	0.26	0.06
Range of RDRR Measurements	0.09 – 0.86	0.09 – 0.86	0.45 – 0.81
NRMSE	**0.32**	**0.33**	**0.20**
Note. The abbreviations GR and SO represent percent gravel and sorting, respectively			

5.3.2 Raivavae and Bora Bora Models

Coral and *Halimeda* showed similar performance for predicting RDRR for Bora Bora as they did for water depth; with an increase in performance within the interior subgroup (Appendix, Table 11). The most accurate model formulated from the Raivavae dataset suitable to be tested on the Bora Bora dataset predicted RDRR based on percent coral and percent *Halimeda* (Table 8). This model had moderate accuracy as applied to Raivavae (NRMSE: platform-wide = 0.24, margin = 0.32, and interior = 0.24). Applying this to Bora Bora yielded equal results for the platform-wide subgroup (NRMSE = 0.24), but less accurate results for the margin and interior subgroups (NRMSE: margin 0.55= and interior = 0.32). Compared to the Raivavae model, the Bora Bora produced equally accurate predictions for the platform-wide subgroup (NRMSE = 0.24), more accurate predictions for the margin subgroup (NRMSE = 0.25), and less accurate predictions for the interior subgroup (NRMSE = 0.26), as seen in Table 9. This model also predicted RDRR based on percent coral and percent *Halimeda*, but had different coefficients than the Raivavae model.

Table 8: Summary of the top selected Raivavae RDRR model suitable to be applied to the Raivavae and Bora Bora datasets. The model was applied to the platform-wide, MARGIN, and INTERIOR subgroups of each dataset. Coefficients of the model vary by subgroup. RMSE of the model is on a scale of 0 – 1, and represents 0% – 100% of total transect length spanning from the reef rim to the central island. NRMSE (in bold) gives the error (on a scale of 0 – 1) of the model for the range of RDRR measurements.

Top Selected Raivavae RDRR Model Suitable to be Applied to Raivavae and Bora Bora				
Subgroup		**Platform-wide**	**Margin**	**Interior**
Model		RDRR = 0.70 - 0.801CR + 0.097HA	RDRR = 1.019 - 1.033CR - 0.953HA	RDRR = 0.645 - 0.809CR + 0.241HA
As Applied to Raivavae	**RMSE**	0.17	0.18	0.15
	Range of RDRR Measurements	0.17 – 0.89	0.17 – 0.72	0.27 – 0.89
	NRMSE	**0.24**	**0.32**	**0.24**
As Applied to Bora Bora	**RMSE**	0.21	0.36	0.22
	Range of RDRR Measurements	0.07 – 0.96	0.07 – 0.73	0.28 – 0.96
	NRMSE	**0.24**	**0.55**	**0.32**
Note. The abbreviations CR and HA represent percent coral and percent *Halimeda*, respectively				

Table 9: Summary of the top selected Bora Bora RDRR model as applied to the platform-wide, margin, and interior subgroups of the Bora Bora dataset. Coefficients of the model vary by subgroup. RMSE of the model is on a scale of 0 – 1, and represents 0% – 100% of total transect length spanning from the reef rim to the central island NRMSE (in bold) gives the error (on a scale of 0 – 1) of the model for the range of RDRR measurements.

Top Selected Bora Bora RDRR Model Applied to Bora Bora			
Subgroup	**Platform-wide**	**Margin**	**Interior**
Model	RDRR = 0.678 – 0.621CR – 0.081HA	RDRR = 0.453 – 0.853CR – 0.758HA	RDRR = 0.697 – 0.316CR – 0.328HA
RMSE	0.21	0.17	0.18
Range of RDRR Measurements	0.07 – 0.96	0.07 – 0.73	0.28 – 0.96
NRMSE	**0.24**	**0.25**	**0.26**
Note. The abbreviations CR and HA represent percent coral and percent *Halimeda*, respectively			

5.4 Sedimentary Properties Can't Reliably Differentiate Between Platform Margin and Platform Interior

5.4.1 Raivavae Linear Discriminant Analysis Model

Box plots for each of the six sedimentary properties were analyzed, and revealed coral and *Halimeda* to have the greatest variance in abundance when comparing between the margin and interior (Fig. 14). Thus, these properties were selected for further analysis using LDA. The resulting LDA model formulated from the Raivavae dataset was:

$$R = 7.924CR - 1.920HA \quad (7)$$

where R is the Raivavae LDA model and CR and HA are the percentage of coral and *Halimeda*, respectively. This model was used as a mathematical boundary line to classify sediment samples as either belonging to the margin or interior environment of deposition based on the abundance of coral and *Halimeda* measured from the sample. The model had an accuracy of 78.57% and 71.43% for the margin and interior of Raivavae, respectively (Fig. 15A). It produced stronger results for the interior samples of Tubuai (accuracy = 83.33%) and Bora Bora (accuracy = 84.21%), but weaker results for the margin samples (accuracy: Tubuai = 46.67% and Bora Bora = 45.45%) (Fig. 15B, C).

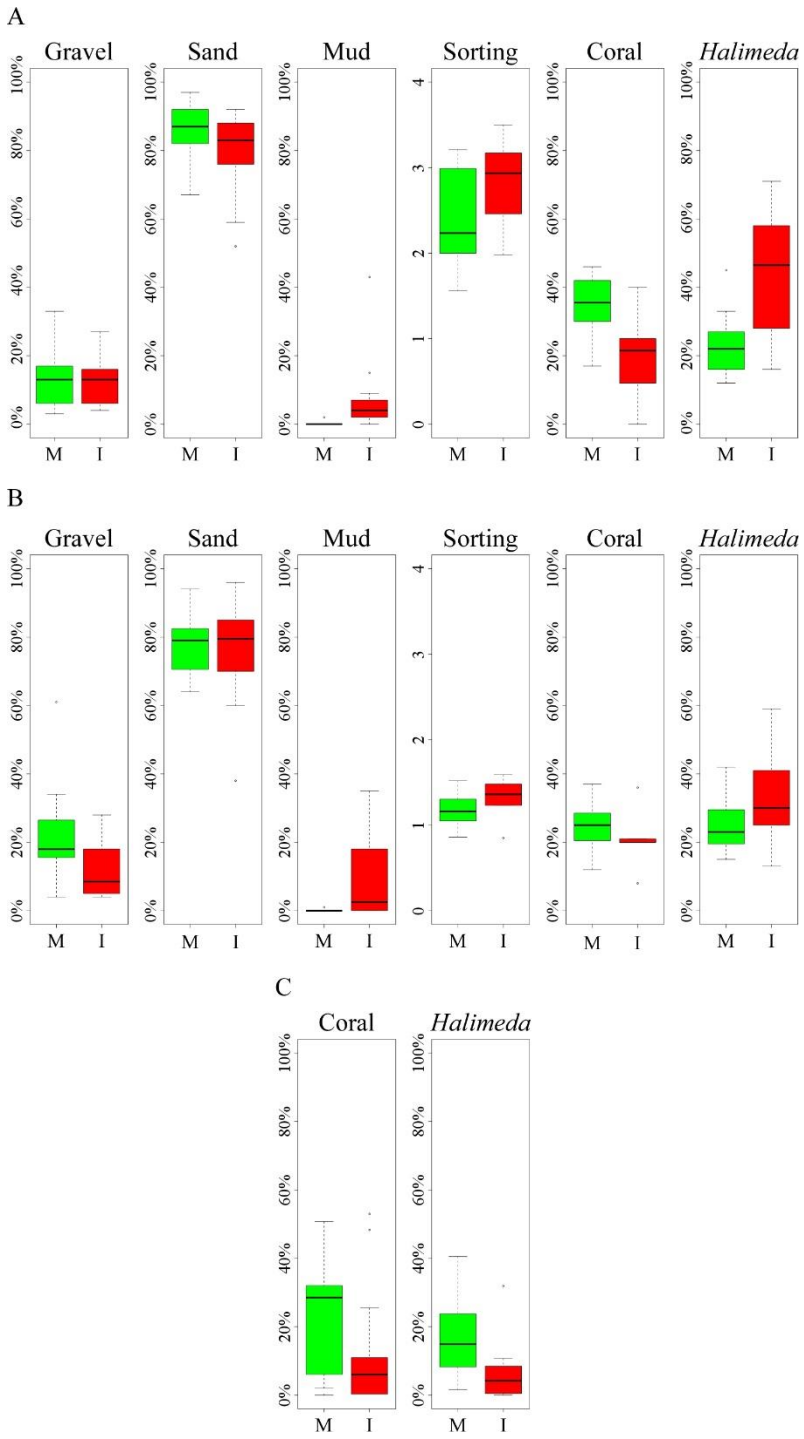

Figure 14: Box plots illustrating the variance in abundance of each sedimentary property between the margin (M) and interior (I) of Raivavae (A), Tubuai (B), and Bora Bora (C). Coral and *Halimeda* showed the greatest variance in abundance between the margin and interior for all three study sites, as illustrated by the degree of separation between the margin and interior box and whiskers for each grain type.

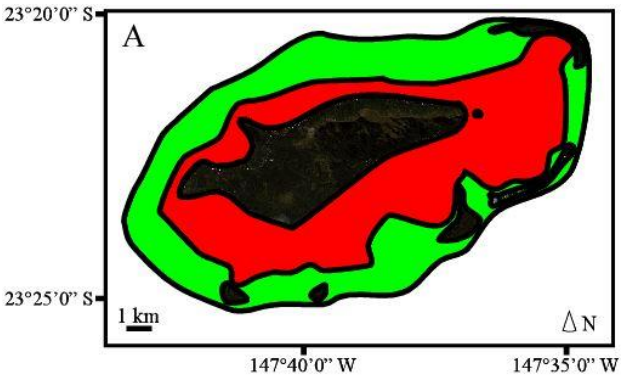

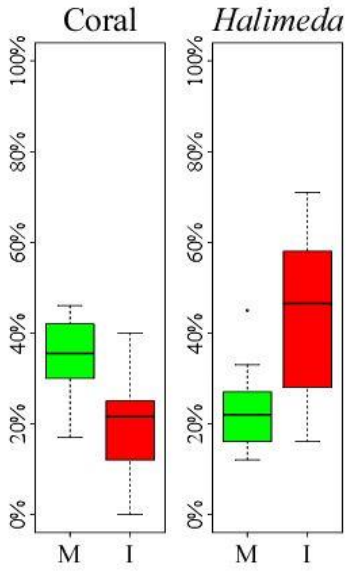

LDA		
	Margin	**Interior**
Margin	**11**	4
Interior	3	**10**
Accuracy	78.57%	71.43%

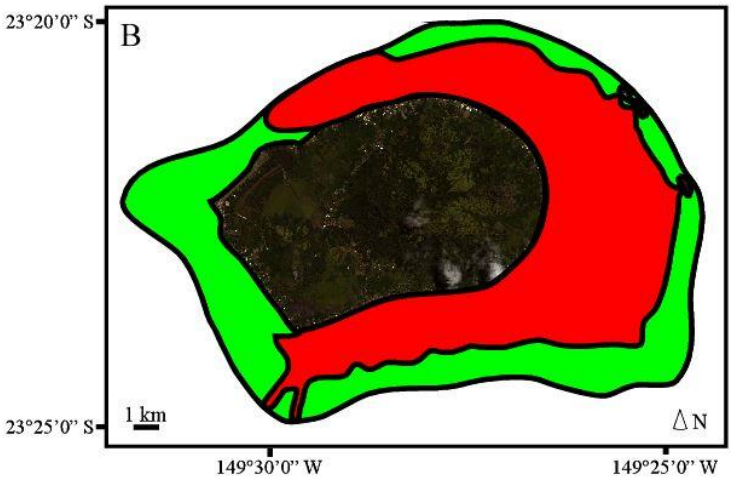

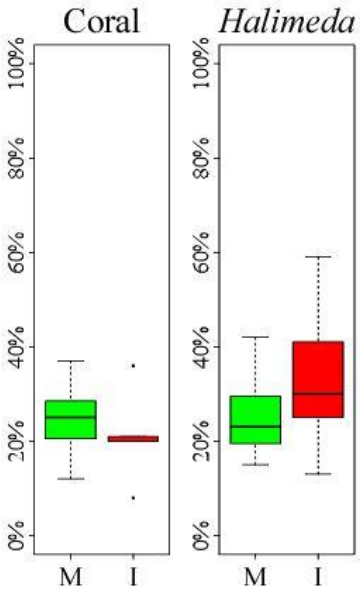

LDA		
	Margin	**Interior**
Margin	**7**	1
Interior	8	**5**
Accuracy	46.67%	83.33%

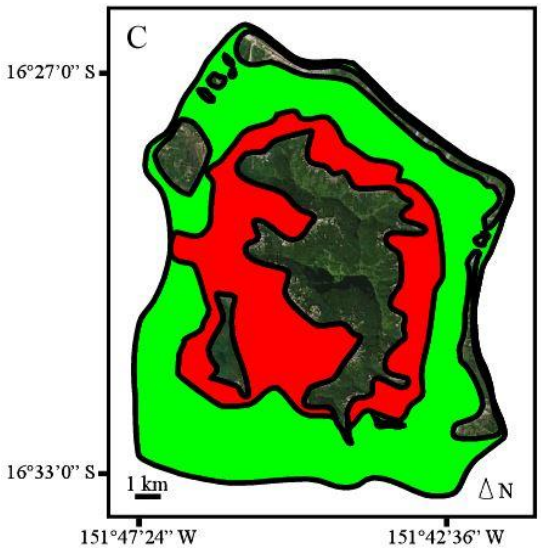

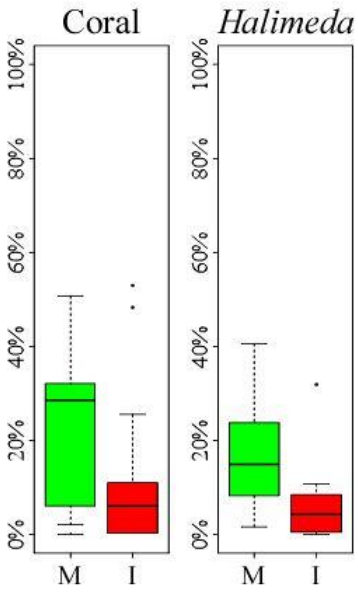

LDA		
	Margin	**Interior**
Margin	**5**	3
Interior	6	**16**
Accuracy	45.45%	84.21%

Figure 15: Representations of the margin (green) and interior (red) drawn over satellite imagery coupled with boxplots that show the abundance of coral and *Halimeda* for the margin (green) and interior (red) of Raivavae (A), Tubuai (B), and Bora Bora (C). Results from applying the LDA model formulated from the Raivavae dataset to each of the three platforms are included in the associated tables. Correct classifications are in bold.

5.4.2 Tubuai and Bora Bora Linear Discriminant Analysis Models

Two other LDA models were formulated using the Tubuai dataset and the Bora Bora dataset. The Tubuai LDA model was:

$$T = -1.766CR - 10.394HA \quad (8)$$

where T is the Tubuai LDA model and CR and HA are the percentage of coral and *Halimeda*, respectively. The Bora Bora LDA model was:

$$B = 1.892CR + 8.688HA \quad (9)$$

where B is the Bora Bora LDA model and CR and HA are the percentage of coral and *Halimeda*, respectively. Again, these models were formulated to classify sediment

samples as either belonging to the margin or interior environment of deposition based on the abundance of coral and *Halimeda* measured from the sample.

The Tubuai LDA model produced strong results for classifying the margin samples (accuracy: Raivavae = 92.86%, Tubuai = 93.33%, and Bora Bora = 90.91%), but poor results for classifying the interior samples (accuracy: Raivavae = 57.14%, Tubuai = 16.67%, and Bora Bora = 0%), as shown in Table 10. Similarly, the Bora Bora specific model produced strong results for the margin samples of Raivavae (accuracy = 92.85%) and Tubuai (accuracy = 100%), and poor results for the interior samples of Raivavae and Tubuai (accuracy: both = 0%) (Table 11). However, it produced stronger results for the interior samples of Bora Bora (accuracy = 84.21%), while producing weaker results for the margin samples of Bora Bora (accuracy = 54.55%). Of the three models that were evaluated (equations 6 – 8), the Raivavae model (equation 6) produced the best overall results for all three datasets (accuracy: Raivavae = 75%, Tubuai = 65%, and Bora Bora = 64.83%).

Table 10: Results from applying the Tubuai LDA model to all three datasets. Correct classifications are in bold.

	Raivavae		**Tubuai**		**Bora Bora**	
	Margin	**Interior**	**Margin**	**Interior**	**Margin**	**Interior**
Margin	**13**	6	**14**	5	**10**	19
Interior	1	**8**	1	**1**	1	**0**
Accuracy	92.86%	57.14%	93.33%	16.67%	90.91%	0.00%

Table 11: Results from applying the Bora Bora LDA model to all three datasets. Correct classifications are in bold.

	Raivavae		**Tubuai**		**Bora Bora**	
	Margin	**Interior**	**Margin**	**Interior**	**Margin**	**Interior**
Margin	**13**	14	**15**	6	**6**	3
Interior	1	**0**	0	**0**	5	**16**
Accuracy	92.86%	0.00%	100.00%	0.00%	54.55%	84.21%

7. Discussion

Results from this study indicate that the selected sedimentary properties can be used to predict water depth and RDRR from the three study sites with moderate accuracy. Generally, water depth was predicted with ≥ 73% accuracy, while RDRR was predicted with ≥ 67% accuracy. Of course, the accuracy of water depth and RDRR predictions varied among and within platforms. In addition, the models selected from each platform as the most applicable were site specific. However, the Raivavae water depth model that used mud and coral as explanatory variables was accurate for both Raivavae (accuracy = 81%) and Tubuai (accuracy = 78%). Percent coral and percent *Halimeda* exhibited similar predictive power when used in the Raivavae LDA model to differentiate between the margin and interior environments (accuracy: Raivavae: 75%, Tubuai = 65%, and Bora Bora = 65%).

The level of accuracy presented by the water depth, RDRR, and LDA models is not surprising. Though most isolated platforms display a general pattern of sediment distribution (i.e. larger, coralgal grains proximal to the reef crest and finer sediments constituted by a mixture of *Halimeda*, mollusk, and forams in the interior), much variation in this pattern has been documented (Masse *et al.*, 1989; Chevillon, 1996; Gischler, 2006; Rankey & Reeder, 2010). The findings of this study present that, on these three platforms, the distribution of sediments shows general trends with water depth and distance from the reef rim. The predictive relationship between sedimentary properties and water depth and distance from the rim is, however, most likely diminished by local environmental effects that govern sediment production, redistribution, and accumulation (e.g. assemblages of sediment producers, wind and wave energy, currents of removal and currents of delivery, bioerosion and bioturbation, tidal velocity, and antecedent topography). These effects vary in extent and duration across the platform top and work together in unique ways to produce complex spatial patterns of sediment distribution among and within isolated platforms (Wright & Burgess, 2005; Rankey *et al.*, 2011; Harris *et al.*, 2014b).

7.1 Apparent Local Environmental Effects

Wave energy, in the form of local wind-driven waves, open ocean swell, and storm surge is a well-documented environmental effect that influences sediment distribution in reef environments (Rankey *et al.*, 2011; Harris *et al.*, 2014a; Wasserman & Rankey, 2014; Purkis *et al.*, 2015b). Wave energy interacts with each platform differently to create among and within platform differences of sediment accumulation. Waves are usually strongest along the windward margin of a platform (Hine *et al.*, 1981); however, distal, open ocean swell may propagate from a direction that is contrary to windward influences and have a greater impact of sediment distribution (Rankey *et al.*, 2009; Wasserman & Rankey, 2014). Raivavae, Tubuai, and Bora Bora are all within the southeast trade wind belt and experience prevailing winds from the east southeast (Wisuki, 2012b, 2012a). In addition, all three of these platforms experience open ocean swell from the south southwest (Wisuki, 2012b, 2012a). The influences from the trade winds and open ocean swell can be observed in the large expanse of the eastern, southern, and western sand aprons of each platform. Though each platform appears to have generally similar windward and swell-ward influences, the distance of each isolated paltform from one another (distance: Raivavae and Tubuai ~ 210 km, Raivavae and Bora Bora ~ 920 km, and Tubuai and Bora Bora ~ 800 km) suggests that each site probably experiences local variations of wind speed and direction and wave direction, height and period that influences the accumulation of sediments in unique ways.

The manner in which local winds and waves interact with each platform and influence sediment distribution is based on the morphology (i.e. size and shape) and orientation of the platform in regards to prevailing winds and waves (Rankey & Garza-Pérez, 2012). The three study sites exhibit a variety of size, shape, and orientation to wind and wave influences. Raivavae is horizontally elongated, with the longest vertical and horizontal axis having approximate dimensions of 7.36 km x 14.33 km. Raivavae is oriented on a slight angle that completely exposes its southern margin to the east southeast prevailing trade winds and associated wind driven waves. Influence from the wind driven waves can be observed in the lagoonward extent of the southern sand apron. The largest extent of which spans about 2 km from reef crest to lagoon. Conversely, Tubuai and Bora Bora are both larger, less horizontally elongated (dimensions: Tubuai ~

10.73 km x 16.69 km and Bora Bora ~ 14.41 km x 9.87 km), and positioned on a north-south orientation. Tubuai has a pronounced western sand apron (max extent ~ 2.5 km) while Bora Bora has a pronounced southern sand apron (max extent ~ 2.5 km). The lagoonward extents of both of these sand aprons are indicative of each platforms exposure to southwestern open ocean swell.

The vertical and lateral extents of sediment accumulations produced by wave and tidal energy can also be influenced by antecedent topography. The series of topographic lows and highs of the antecedent topography act as sinks and barriers to sediment accumulation, and as conduits and barriers to current flow (Rankey *et al.*, 2009; Harris *et al.*, 2014a; Isaack & Gischler, 2015). The antecedent topography of a platform is a factor of subaerial solution (karstification) of the bedrock subsurface during periods of sea-level lowstands and differential accretion rates of platform margins and interiors (Schlager, 1993; Purdy & Winterer, 2001; Gischler, 2015). The degree of karstification is dictated by subsidence rates and precipitation, which differs among platforms (Isaack & Gischler, 2015). The distinctive antecedent topography of each platform creates a unique landscape for sediment accumulation. Though there is no data to reveal the structure and subsequent influence of antecedent topography on the three study sites, inferences can be made from observations of lagoonal depth and the topographic highs and lows on the platform tops of Raivavae, Tubuai, and Bora Bora (Isaack & Gischler, 2015).

The combined effects of wind and wave energy, platform morphology and orientation, and antecedent topography influence platform currents. Platform currents that are strengthened by wind/wave activity, tides, and/or connectivity to stronger, open ocean currents can be strong enough to transport sediments in the platform margin and interior (Kench, 1998a; Kench, 1998b; Gischler, 2006; Rankey & Reeder, 2010; Harris *et al.*, 2014a). No data for the platform currents of the study sites was used, but inferences can be made from spatial patterns of sediment grain size and from close inspection of satellite imagery of each site. Gischler (2011) reports a high abundance (mean = 70%) of fines ($s < 0.125$ mm) in the interior of Bora Bora interpreted to be derived from the breakdown of skeletal fragments. Conversely, mud was ubiquitously low in the interior of Raivavae and Tubuai. The lack of mud on Raivavae and Tubuai indicates a lack of production of fine

grains and/or a high-energy environmental setting. Nothing can be said regarding the production of mud on Raivavae and Tubuai; however, there are hints of a high-energy lagoonal environment on both platforms, which could account for the similarities in grain texture and faunal grain type between the interior and margin environments of these two sites.

Raivavae and Tubuai both have a prominent pass in the northern reef rim and smaller passes in the southern reef rim that allow for improved hydrodynamic connectivity between the open-ocean and lagoon. Close inspection of satellite imagery for Raivavae and Tubuai reveals markings in the lagoon floor indicative of current flow around the central island of each platform (Figs. 16 and 17). It is highly likely that the currents in the lagoon of Raivavae and Tubuai are strong enough to winnow mud from the lagoon. Gischler (2011) states that lagoonal circulation on Bora Bora is characterized by water entering the lagoon via reef spill over and exiting through the Ava Nui channel in the west. The lagoon of Bora Bora is substantially deeper than that of Raivavae and Tubuai (depth: Bora Bora ~ 40 m and Raivavae and Tubuai ~ 20 m), and is broken up into six basins. The reduced circulation caused by a combination of minimal lagoonal input of open ocean water and a deep, disjointed lagoon creates a tranquil lagoonal environment virtually devoid of strong currents and thus an ideal setting for the accumulation of fine grains.

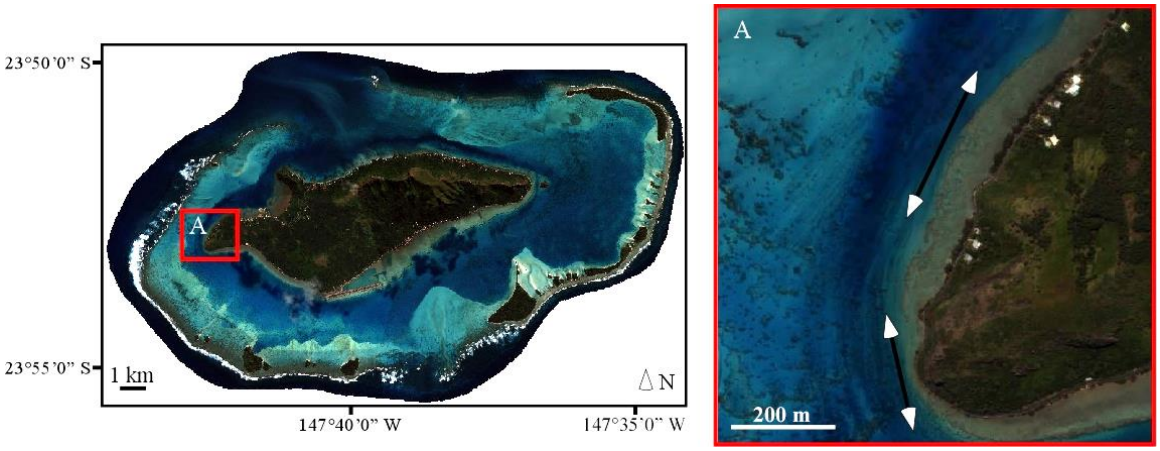

Figure 16: WorldView-2 satellite imagery of Raivavae. Subscene (A) provides a close up highlighting sedimentary bedforms on the lagoon floor that may be indicative of current flow around the central island of Raivavae. The lines with double arrows illustrate the possible current directions around the central island as interpreted from the satellite imagery.

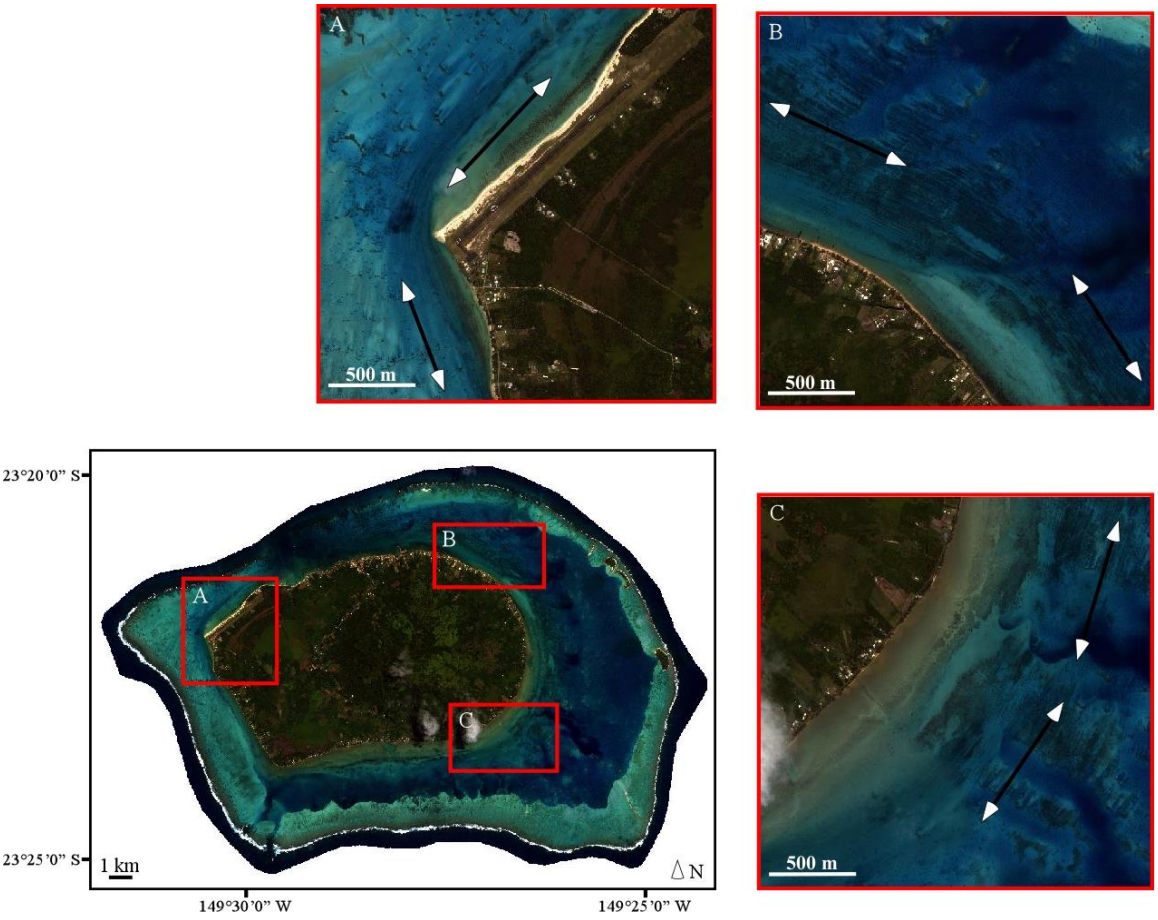

Figure 17: WorldView-2 satellite imagery of Tubuai. Subscenes (A, B, and C) provide a close ups showing sedimentary bedforms on the lagoon floor that may be indicative of current flow around the central island of Tubuai. The lines with double arrows illustrate the possible current directions around the central island as interpreted from the satellite imagery.

Another major effect that contributes to the complexity of sediment production, transportation and re-distribution is the assemblages of grain producers. In addition to being produced on the platform margin, carbonate sediment can be produced in situ within the back reef sand apron and lagoon. Major contributors to carbonate production in these environments include: coral patch reefs, bivalve and gastropod fragments, *Halimeda* plates and other calcareous green algae, and certain varieties of forams (Adjas *et al.*, 1990; Yamano *et al.*, 2002; Gischler, 2011). *In situ* production from these contributors directly impacts the grain texture and type by adding non-reef derived

sediment that is not in equilibrium with the surrounding ambient hydrodynamics (Wasserman & Rankey, 2014). Close observations of satellite imagery available for the three study sites shows that the lagoons of Raivavae and Tubuai have a substantial number of patch reefs within the back reef apron and lagoon; however, Gischler (2011) reports a scarcity of patch reefs in the lagoon of Bora Bora. It is highly plausible that *in situ* production of sediment from lagoonal patch reefs and other sediment producers coupled with differential patterns of hydrodynamics, influenced by local wave patterns and platform morphology and orientation, are the main forces behind the unique patterns of sediment production, redistribution and accumulation apparent on each study site. The unique patterns, inherent to each platform, help explain the reduced level of accuracy and the among and within platform differences observed in the water depth, RDRR, and LDA models

7.2 Abundance of Coral Fragments: Indicator of Distance from Reef Rim with Applications to the Rock Record

Results from Raivavae and Bora Bora show that the abundance of coral holds potential to be an indicator of distance from the reef rim. In addition to being a variable in the top selected water depth and RDRR models for Raivavae, coral was a reoccurring variable in nine of the top 15 (five for each subgroup) water depth models and 10 of the top 15 (five for each subgroup) RDRR models for Raivavae. On these study sites water depth generally increases with increasing distance from the reef rim. Consequently, the relationship between coral and water depth as seen in the models also has impactions to distance from the reef rim. The recurrence of coral in the top Raivavae models and the accuracy of the top selected Raivavae and Bora Bora water depth and RDRR models suggest that coral is a primary feature linked to RDRR.

The zonation of coral reefs and their associated detritus make the abundance of coral a suitable proxy to estimate the distance from the reef rim (Rankey *et al.*, 2011; Wasserman & Rankey, 2014). Coral grows in highest abundance on the platform margin. Here, wave energy stirs up nutrients and flushes out waste and suspended sediment, providing the ideal environment for corals (Scholle & Ulmer-Scholle, 2003; Schlager & Purkis, 2013). Carbonate grains are generally deposited in close proximity to their

environment of origin, consequently a high abundance of coral fragments can be found on the platform margin and back reef sand apron (Masse *et al.*, 1989; Gischler & Lomando, 1999; Gischler, 2006, 2011). Further lagoonward, wave energy dissipates and depth increases; causing water quality and clarity to decrease and become less favorable for coral. In result, the abundance of coral declines and is reflected in the surrounding sediment (Ginsburg, 1956; Purdy, 1963; Milliman, 1967; Gischler & Lomando, 1999). Lagoonal patch reefs are an exception. They contribute coral fragments to lagoonal sediments, but the abundance of coral fragments dissipates with distance from patch reefs (Tudhope *et al.*, 1985). The presence of patch reefs provides variability in the trend between distance from the reef rim and abundance of coral fragments; however, coral rich sediments can still be considered generally reliable indicators of proximity to the reef rim.

The relationship between distance from the reef rim and abundance of coral also has implications to the rock record. Modern scleractinian corals have been major contributors to reef framework, and thus carbonate platforms, since the Miocene (~ 23 MA) (Scholle & Ulmer-Scholle, 2003; Flügel, 2004). Ancient carbonate platforms are of particular interest given their propensity to form excellent water aquifers and hydrocarbon reservoirs. Sampling ancient platforms to describe their dimensional anatomy and locate reservoirs is a difficult task that often involves interpreting lateral facies heterogeneity from drilled rock cores collected from sparsely spaced wells, or from analyzing vertical and horizontal facies changes within an outcrop. The relationship between distance from the reef rim and coral abundance, as seen from the modern examples presented in this study, may provide a tool to better interpret lateral facies heterogeneity and predict locations of potential Miocene-age reservoirs based on core samples.

8. Conclusion

In summary, this study revealed that on Raivavae, Tubuai, and Bora Bora, sediment texture and type can be used to predict water depth and distance from the reef rim and differentiate between marginal and interior environments with moderate accuracy ($\geq 65\%$). Among and within platform differences observed in water depth and RDRR

models prevented the application of a single model to more than one platform. The exception being the Raivavae water depth model that predicted water depth on a platform-wide scale based on the abundance of mud and coral. This model had an accuracy of 81% and 78% when applied to Raivavae and Tubuai, respectively. The overall reduced level of model accuracy and the among and within platform differences of the models were likely due to several local effects that influence sediment production, redistribution, and accumulation that produced unique sedimentary patterns among and within platforms. Overall, the results of this study suggest that the abundance of coral holds potential to be utilized as a proxy for distance from the reef rim on modern and ancient isolated carbonate platforms.

To expand the applicability of the modeling performed in this study, future studies should incorporate data from a larger swath of isolated platforms. Ideally, a more thorough sampling scheme should be implemented as well. Sampling transects should have multiple sediment sample locations and span from the reef rim to central lagoon. The entirety of the platform should be sampled if possible. Investigations into windward/swell-ward and leeward differences and analyzing models that capture these differences could be performed with a more thoroughly sampled dataset.

9. References

Adjas, A., Masse, J.-P., & Montaggioni, L. F. (1990). Fine-grained carbonates in nearly closed reef environments: Mataiva and Takapoto atolls, Central Pacific Ocean. *Sedimentary Geology, 67*(1), 115-132.

Babyak, M. A. (2004). What you see may not be what you get: a brief, nontechnical introduction to overfitting in regression-type models. *Psychosomatic medicine, 66*(3), 411-421.

Betzler, C., Lindhorst, S., Eberli, G. P., Lüdmann, T., Möbius, J., Ludwig, J., . . . Hübscher, C. (2014). Periplatform drift: The combined result of contour current and off-bank transport along carbonate platforms. *Geology, 42*(10), 871-874.

Blott, S. J., & Pye, K. (2001). GRADISTAT: a grain size distribution and statistics package for the analysis of unconsolidated sediments. *Earth surface processes and Landforms, 26*(11), 1237-1248.

Bosence, D. (2008). Randomness or order in the occurrence and preservation of shallow-marine carbonate facies? Holocene, South Florida. *Palaeogeography, Palaeoclimatology, Palaeoecology, 270*(3), 339-348.

Braga, J. C., Martín, J. M., & Riding, R. (1996). Internal structure of segment reefs: Halimeda algal mounds in the Mediterranean Miocene. *Geology, 24*(1), 35-38.

Burnham, K. P., & Anderson, D. R. (2002). *Model selection and multimodel inference: a practical information-theoretic approach*: Springer.

Chevillon, C. (1996). Skeletal composition of modern lagoon sediments in New Caledonia: coral, a minor constituent. *Coral Reefs, 15*(3), 199-207.

Eberli, G. P. (1989). Cenozoic progradation of northwestern Great Bahama Bank, a record of lateral platform growth and sea-level fluctuations.

Fisher, R. A. (1936). The use of multiple measurements in taxonomic problems. *Annals of eugenics, 7*(2), 179-188.

Flügel, E. (2004). *Microfacies of carbonate rocks: analysis, interpretation and application*: Springer.

Folk, R. L., & Ward, W. C. (1957). Brazos River bar: a study in the significance of grain size parameters. *Journal of Sedimentary Research, 27*(1).

Ginsburg, R. N. (1956). Environmental relationships of grain size and constituent particles in some south Florida carbonate sediments. *AAPG bulletin, 40*(10), 2384-2427.

Gischler, E. (2006). Sedimentation on Rasdhoo and Ari Atolls, Maldives, Indian Ocean. *Facies, 52*(3), 341-360.

Gischler, E. (2011). Sedimentary facies of Bora Bora, Darwin's type barrier reef (Society Islands, south Pacific): the unexpected occurrence of non-skeletal grains. *Journal of Sedimentary Research, 81*(1), 1-17.

Gischler, E. (2015). Quaternary reef response to sea - level and environmental change in the western Atlantic. *Sedimentology, 62*(2), 429-465.

Gischler, E., & Lomando, A. J. (1999). Recent sedimentary facies of isolated carbonate platforms, Belize-Yucatan system, Central America. *Journal of Sedimentary Research, 69*(3).

Gischler, E., & Zingeler, D. (2002). The origin of carbonate mud in isolated carbonate platforms of Belize, Central America. *International Journal of Earth Sciences, 91*(6), 1054-1070.

Harris, D. L., Vila-Concejo, A., & Webster, J. M. (2014a). Geomorphology and sediment transport on a submerged back-reef sand apron: One Tree Reef, Great Barrier Reef. *Geomorphology, 222*, 132-142.

Harris, P., Purkis, S., Ellis, J., Swart, P., & Reijmer, J. (2014b). Mapping water-depth and depositional facies on Great Bahama Bank. *Sedimentology*.

Harris, P., & Vlaswinkel, B. (2008). Modern isolated carbonate platforms: Templates for quantifying facies attributes of hydrocarbon reservoirs. *Controls on carbonate platform and reef development: SEPM Special Publication, 89*, 323-341.

Harris, P. M. (1979). *Facies anatomy and diagenesis of a Bahamian ooid shoal* (Vol. 7): Comparative Sedimentology Laboratory, Division of Marine Geology and Geophysics, University of Miami, Rosenstiel School of Marine & Atmospheric Science.

Harris, P. M. (1983). The Joulters ooid shoal, Great Bahama Bank *Coated Grains* (pp. 132-141): Springer.

Harris, P. M. M., Purkis, S. J., & Ellis, J. (2011). Analyzing spatial patterns in modern carbonate sand bodies from Great Bahama Bank. *Journal of Sedimentary Research, 81*(3), 185-206.

Hillis-Colinvaux, L. (1980). Ecology and taxonomy of Halimeda: primary producer of coral reefs. *Advances in marine biology, 17*, 1-327.

Hine, A. C., Wilber, R. J., & Neumann, A. C. (1981). Carbonate sand bodies along contrasting shallow bank margins facing open seaways in northern Bahamas. *AAPG bulletin, 65*(2), 261-290.

Illing, L. V. (1954). Bahaman calcareous sands. *AAPG bulletin, 38*(1), 1-95.

Imbrie, J., & Purdy, E. G. (1962). Classification of modern Bahamian carbonate sediments.

Isaack, A., & Gischler, E. (2015). The significance of sand aprons in Holocene atolls and carbonate platforms. *Carbonates and Evaporites*, 1-13.

Kaczmarek, S. E., Hicks, M. K., Fullmer, S. M., Steffen, K. L., & Bachtel, S. L. (2010). Mapping facies distributions on modern carbonate platforms through integration of multispectral Landsat data, statistics-based unsupervised classifications, and surface sediment data. *AAPG bulletin, 94*(10), 1581-1606.

Kench, P. (1998a). A currents of removal approach for interpreting carbonate sedimentary processes. *Marine Geology, 145*(3), 197-223.

Kench, P. S. (1998b). Physical controls on development of lagoon sand deposits and lagoon infilling in an Indian Ocean atoll. *Journal of Coastal Research*, 1014-1024.

Kohler, K. E., & Gill, S. M. (2006). Coral Point Count with Excel extensions (CPCe): A Visual Basic program for the determination of coral and substrate coverage using random point count methodology. *Computers & Geosciences, 32*(9), 1259-1269.

Lachenbruch, P. A., & Mickey, M. R. (1968). Estimation of error rates in discriminant analysis. *Technometrics, 10*(1), 1-11.

Madden, R. H., Wilson, M. E., & O'Shea, M. (2013). Modern fringing reef carbonates from equatorial SE Asia: An integrated environmental, sediment and satellite characterisation study. *Marine Geology, 344*, 163-185.

Masse, J., Thomassin, B., & Acquaviva, M. (1989). Bioclastic sedimentary environments of coral reefs and lagoon around Mayotte island (Comoro archipelago, Mozambique channel, SW Indian Ocean). *Journal of Coastal Research*, 419-432.

McLachlan, G. (2004). *Discriminant analysis and statistical pattern recognition* (Vol. 544): John Wiley & Sons.

Milliman, J. D. (1967). Carbonate sedimentation on Hogsty Reef, a Bahamian atoll. *Journal of Sedimentary Research, 37*(2).

Montaggioni, L. F. (2005). History of Indo-Pacific coral reef systems since the last glaciation: development patterns and controlling factors. *Earth-Science Reviews, 71*(1), 1-75.

Purdy, E. G. (1963). Recent calcium carbonate facies of the Great Bahama Bank. 2. Sedimentary facies. *The Journal of Geology*, 472-497.

Purdy, E. G., & Winterer, E. L. (2001). Origin of atoll lagoons. *Geological Society of America Bulletin, 113*(7), 837-854.

Purkis, S., Casini, G., Hunt, D., & Colpaert, A. (2015a). Morphometric patterns in Modern carbonate platforms can be applied to the ancient rock record: Similarities between Modern Alacranes Reef and Upper Palaeozoic platforms of the Barents Sea. *Sedimentary Geology, 321,* 49-69.

Purkis, S., Kerr, J., Dempsey, A., Calhoun, A., Metsamaa, L., Riegl, B., . . . Renaud, P. (2014). Large-scale carbonate platform development of Cay Sal Bank, Bahamas, and implications for associated reef geomorphology. *Geomorphology*.

Purkis, S., Vlaswinkel, B., & Gracias, N. (2012a). Vertical-To-Lateral Transitions Among Cretaceous Carbonate Facies—A Means To 3-D Framework Construction Via Markov Analysis. *Journal of Sedimentary Research, 82*(4), 232-243.

Purkis, S. J., & Harris, P. M. M. (2016). The Extent and Patterns of Sediment Filling of Accommodation Space On Great Bahama Bank. *Journal of Sedimentary Research, 86*(4), 294-310.

Purkis, S. J., Harris, P. M. M., & Ellis, J. (2012b). Patterns of sedimentation in the contemporary Red Sea as an analog for ancient carbonates in rift settings. *Journal of Sedimentary Research, 82*(11), 859-870.

Purkis, S. J., Kohler, K. E., Riegl, B. M., & Rohmann, S. O. (2007). The statistics of natural shapes in modern coral reef landscapes. *The Journal of Geology, 115*(5), 493-508.

Purkis, S. J., Riegl, B. M., & Andréfouët, S. (2005). Remote sensing of geomorphology and facies patterns on a modern carbonate ramp (Arabian Gulf, Dubai, UAE). *Journal of Sedimentary Research, 75*(5), 861-876.

Purkis, S. J., Rowlands, G. P., & Kerr, J. M. (2015b). Unravelling the influence of water depth and wave energy on the facies diversity of shelf carbonates. *Sedimentology*.

Purkis, S. J., & Vlaswinkel, B. (2012). Visualizing lateral anisotropy in modern carbonates. *AAPG bulletin, 96*(9), 1665-1685.

Rankey, E. C. (2004). On the interpretation of shallow shelf carbonate facies and habitats: how much does water depth matter? *Journal of Sedimentary Research, 74*(1), 2-6.

Rankey, E. C., & Garza-Pérez, J. R. (2012). Seascape metrics of shelf-margin reefs and reef sand aprons of Holocene carbonate platforms. *Journal of Sedimentary Research, 82*(1), 57-75.

Rankey, E. C., Guidry, S. A., Reeder, S. L., & Guarin, H. (2009). Geomorphic and sedimentologic heterogeneity along a Holocene shelf margin: Caicos Platform. *Journal of Sedimentary Research, 79*(6), 440-456.

Rankey, E. C., & Reeder, S. L. (2010). Controls on platform - scale patterns of surface sediments, shallow Holocene platforms, Bahamas. *Sedimentology, 57*(6), 1545-1565.

Rankey, E. C., & Reeder, S. L. (2011). Holocene oolitic marine sand complexes of the Bahamas. *Journal of Sedimentary Research, 81*(2), 97-117.

Rankey, E. C., Reeder, S. L., & Garza-Pérez, J. R. (2011). Controls On Links Between Geomorphical and Surface Sedimentological Variability: Aitutaki and Maupiti Atolls, South Pacific Ocean. *Journal of Sedimentary Research, 81*(12), 885-900.

Rees, S. A., Opdyke, B. N., Wilson, P. A., & Fifield, L. K. (2005). Coral reef sedimentation on Rodrigues and the Western Indian Ocean and its impact on the carbon cycle. *Philosophical Transactions of the Royal Society A: Mathematical, Physical and Engineering Sciences, 363*(1826), 101-120.

Reijmer, J. J., Swart, P. K., Bauch, T., Otto, R., Reuning, L., Roth, S., & Zechel, S. (2012). A Re - Evaluation of Facies on Great Bahama Bank I: New Facies Maps of Western Great Bahama Bank. *Perspectives in Carbonate Geology: A Tribute to the Career of Robert Nathan Ginsburg (Special Publication 41 of the IAS), 98*, 29-46.

Riegl, B., Halfar, J., Purkis, S., & Godinez-Orta, L. (2007). Sedimentary facies of the eastern Pacific's northernmost reef-like setting (Cabo Pulmo, Mexico). *Marine Geology, 236*(1), 61-77.

Schlager, W. (1993). Accommodation and supply—a dual control on stratigraphic sequences. *Sedimentary Geology, 86*(1), 111-136.

Schlager, W. (2007). *Carbonate Sedimentology and Sequence Stratigraphy* (Vol. 8): SEPM Soc for Sed Geology.

Schlager, W., & Purkis, S. J. (2013). Bucket structure in carbonate accumulations of the Maldive, Chagos and Laccadive archipelagos. *International Journal of Earth Sciences, 102*(8), 2225-2238.

Scholle, P. A., & Ulmer-Scholle, D. S. (2003). *A Color Guide to the Petrography of Carbonate Rocks: Grains, Textures, Porosity, Diagenesis, AAPG Memoir 77* (Vol. 77): AAPG.

Team, R. C. (2014). R: A Language and Environment for Statistical Computing.

Triffleman, N. J., Hallock, P., & Hine, A. C. (1992). Morphology, sediments, and depositional environments of a small carbonate platform; Serranilla Bank, Nicaraguan Rise, Southwest Caribbean Sea. *Journal of Sedimentary Research, 62*(4), 591-606.

Tucker, M. E., & Wright, V. P. (2009). *Carbonate sedimentology*: John Wiley & Sons.

Tudhope, A., Scoffin, T., Stoddart, D., & Woodroffe, C. (1985). *Sediments of Suwarrow atoll.* Paper presented at the Proc 5th Int Coral Reef Symp.

Wasserman, H. N., & Rankey, E. C. (2014). Physical Oceanographic Influences On Sedimentology of Reef Sand Aprons: Holocene of Aranuka Atoll (Kiribati), Equatorial Pacific. *Journal of Sedimentary Research, 84*(7), 586-604.

Weber, J. N., & Woodhead, P. M. (1972). *Carbonate lagoon and beach sediments of Tarawa Atoll, Gilbert Islands*: Smithsonian Institution.

Wetcher-Hendricks, D. (2011). *Analyzing quantitative data: An introduction for social researchers*: John Wiley & Sons.

Wilber, R. J., Milliman, J. D., & Halley, R. B. (1990). Accumulation of bank-top sediment on the western slope of Great Bahama Bank: rapid progradation of a carbonate megabank. *Geology, 18*(10), 970-974.

Wisuki. (2012a). Bora-Bora Statistics. Retrieved 2013, 1 Jun, from http://wisuki.com/statistics/3883/bora-bora

Wisuki. (2012b). Tubuai Statistics. Retrieved 1 Jun, 2013, from http://wisuki.com/statistics/3900/tubuai.

Wright, V. P., & Burgess, P. M. (2005). The carbonate factory continuum, facies mosaics and microfacies: an appraisal of some of the key concepts underpinning carbonate sedimentology. *Facies, 51*(1-4), 17-23.

Yamano, H., Kayanne, H., Matsuda, F., & Tsuji, Y. (2002). Lagoonal facies, ages, and sedimentation in three atolls in the Pacific. *Marine Geology, 185*(3), 233-247.

Appendix A: Photolog of Faunal Grain Types

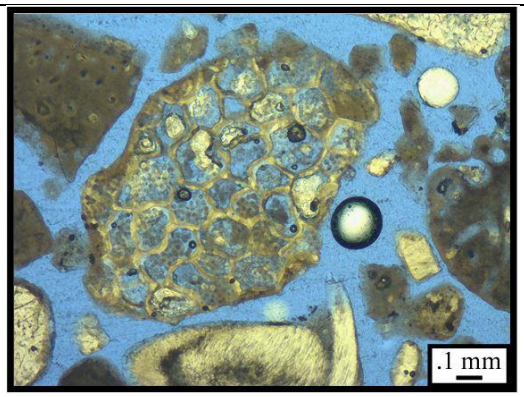

Bryozoan (thin section): colonial with many small, boxy pores, or zooecial apertures, where bryozoan polyps once lived. The main difference between bryozoans and coral are smaller colony size and individual living chambers (Scholle and Ulmer-Scholle 2003).

Bryozoan (loose grain): bryozoans have a similar porous external structure to corals, but at a smaller scale. Compare this picture with the picture of loose coral grains below.

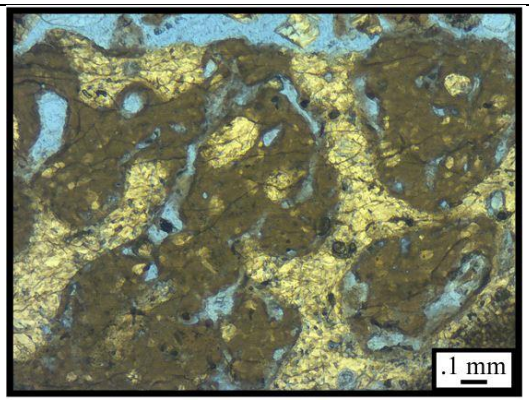

Coral (thin section): colonial with many pores, corallites, where coral polyps once lived. The yellow white is the coral skeleton while the brown is fine grained mud, or matrix, that filled the interstitial space between the skeleton.

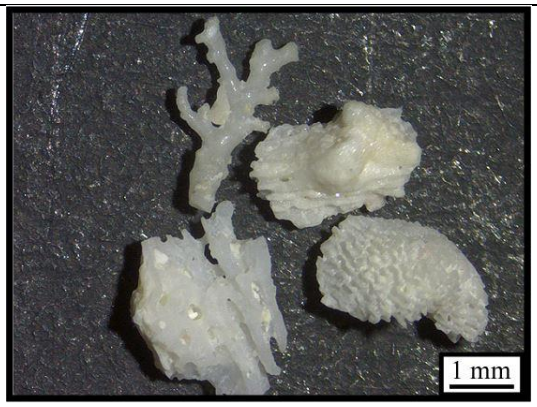

Coral (loose grains): coral fragments may be in many forms: from branching (top left) to more mound like (other grains) each with numerous corallites. Horizontal tabulae and vertical corallite walls create the cell-like internal structure of the coral skeleton.

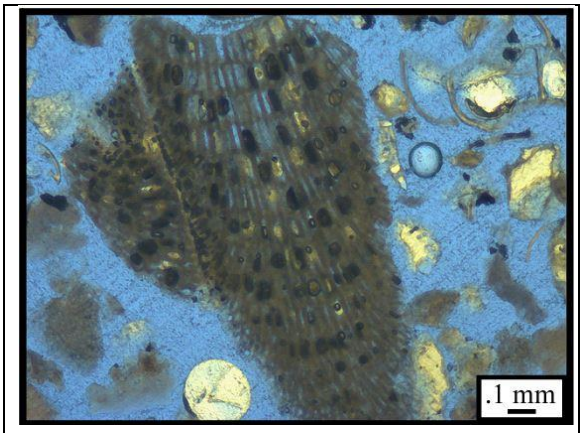

Coralline Red Algae (thin section): brown grain with fine scale reticulate latticework internal structure that reflects the filamentous morphology of this algae (Scholle and Ulmer-Scholle 2003).

Coralline Red Algae (loose grain): no example

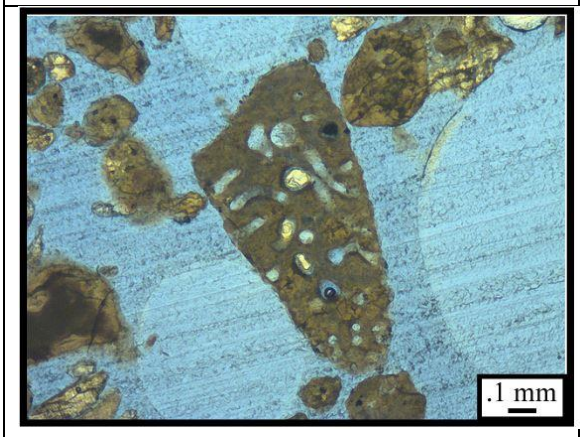

Halimeda (thin section): brown grain porous internal structure. The internal structure is a result of complexly intertwined filaments (Scholle and Ulmer-Scholle 2003).

Halimeda (thin section): larger club shaped grain. The outside layer of the grain may be smooth or covered in tiny pores, or utricles. The internal structure is heavily reticulated.

Mollusk (thin section): gastropods (above) are noted by their strongly curved and smooth shape. Larger, whole specimens have a spiral shape. Bivalves (not pictured) typically appear as thin slightly curved fragments.

Mollusk (loose grains): gastropods (top left and bottom) and mollusks (top right) are easily identifiable. Gastropods have a spiral structure while bivalves appear as single slightly curved shell fragments.

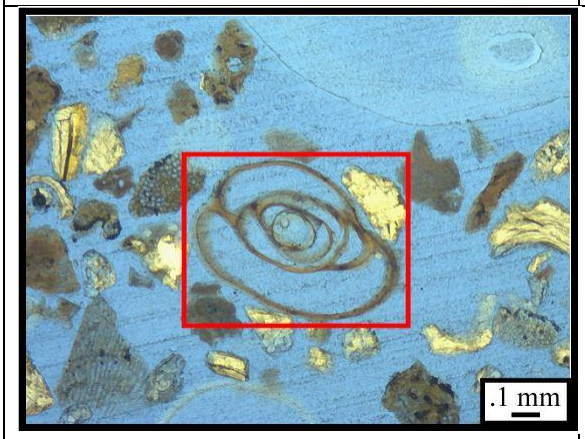

Foram (thin section): most foram tests, outer shell, (boxed in red) are multichambered and can resemble a mollusk shell. However, foram tests are usually much smaller than mollusk shells. Compare scale of above photo.

Foram (loose grains): small tests, usually with a shiny appearance. There are a variety of test morphologies. Above are the most common types found from Raivavae and Tubuai. Tests of these forams are small and flat with a circular shape. Most appear as full tests.

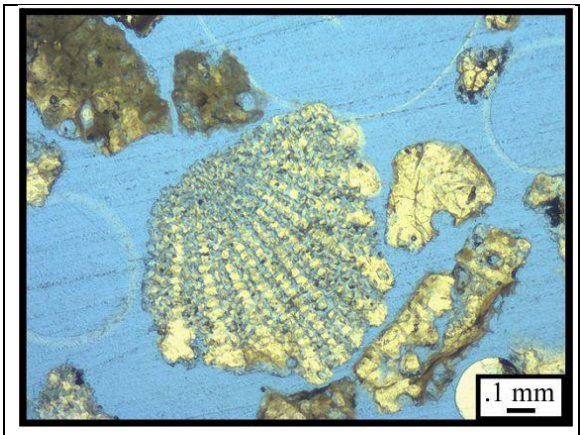

Echinoderm (thin section): echinoderm spines (above) and plates (not pictured) are perforated with a meshwork of honeycomb-like pores. Transversely cut spines are circular with radial symmetry, while a longitudinal sections show long, slender spines with a striped pattern of pore space. The most distinguishing characteristic of echinoderms is their visible extinction of internal structures when viewed with cross polarized light (Scholle and Ulmer-Scholle 2003).

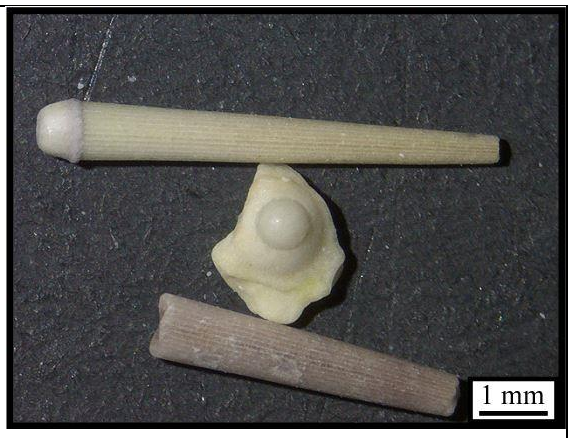

Echinoderm (loose grains): appear as spines (top and bottom) or plates (center) Spines are long and slender and often have a striped pattern. The base of a spine has a collar followed by a ball-like structure that attaches the spine to the plate. The plate (center) shows the spine attachment point as a prominent ball-like structure. Echinoderm plates have a very fine porous structure.

Spicule (thin section): no example	 Spicule (loose grains): calcareous structures found in the tissue of octocorals. Spicules are small spindle-shaped rods with pointed ends and small protrusions or spines (Scholle and Ulmer-Scholle 2003).
Serpulid (thin section): no example	 Serpulid (loose grain): small slender tube typically encrusting upon other grains, but can be found as a solitary structure as well (above).

Crustacean (thin section): no example	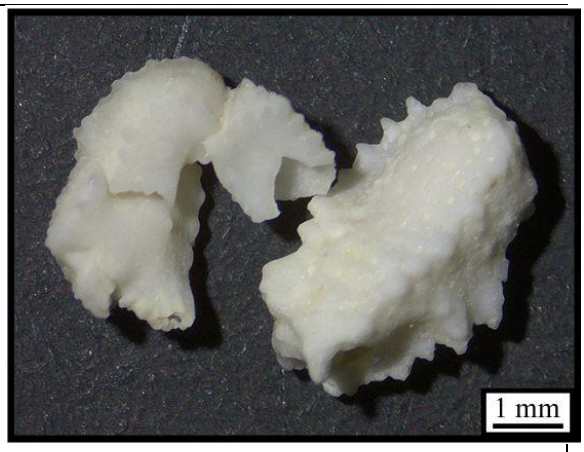 Crustacean (loose grains): fragments of the crustacean exoskeleton. Above are the appendages from a crab exoskeleton. Notable by jointed appendages.

Appendix B: Referenced Tables

Table 1: Sample ID, location, in terms of (margin or interior), RDRR, water depth, percent gravel, percent sand, percent mud, and sorting values of each of the sediment samples collected from the platform top of Raivavae.

Raivavae							
Sample	Location	RDRR	Depth (m)	Gravel	Sand	Mud	Sorting
FPA-8	Interior	0.27	4.21	14.00%	79.00%	7.00%	3.39
FPA-17	Interior	0.33	3.52	6.00%	90.00%	4.00%	2.46
FPA-16	Interior	0.35	4.41	15.00%	83.00%	2.00%	2.79
FPA-11	Interior	0.4	6.48	4.00%	92.00%	5.00%	1.98
FPA-20	Interior	0.49	4.86	8.00%	83.00%	9.00%	2.65
FPA-26	Interior	0.49	7.76	27.00%	59.00%	15.00%	3.08
FPA-22	Interior	0.64	8.21	20.00%	74.00%	7.00%	3.5
FPA-19	Interior	0.67	7.06	5.00%	52.00%	43.00%	3.18
FPA-6	Interior	0.67	4.76	16.00%	83.00%	1.00%	2.93
FPA-28	Interior	0.71	8.28	11.00%	88.00%	1.00%	3.13
FPA-13	Interior	0.76	5.18	13.00%	87.00%	0.00%	2.21
FPA-29	Interior	0.76	10.79	13.00%	82.00%	4.00%	3.17
FPA-2	Interior	0.82	14.88	6.00%	90.00%	3.00%	2.46
FPA-10	Interior	0.89	6.8	20.00%	76.00%	3.00%	2.94
FPA-9	Margin	0.17	2.56	30.00%	70.00%	0.00%	2.01
FPA-24	Margin	0.2	1.23	23.00%	77.00%	0.00%	2.99
FPA-25	Margin	0.21	0.72	16.00%	84.00%	0.00%	3.04
FPA-1	Margin	0.29	4.37	3.00%	97.00%	0.00%	1.59
FPA-18	Margin	0.34	1.48	33.00%	67.00%	0.00%	3.03
FPA-21	Margin	0.36	1.42	13.00%	87.00%	0.00%	2.19
FPA-12	Margin	0.39	1.36	17.00%	82.00%	0.00%	2.6
FPA-30	Margin	0.43	1.98	5.00%	92.00%	2.00%	3.21
FPA-15	Margin	0.44	1.22	12.00%	88.00%	0.00%	2
FPA-14	Margin	0.56	1.55	14.00%	85.00%	0.00%	2.26
FPA-23	Margin	0.59	1.97	10.00%	90.00%	0.00%	2.95
FPA-3	Margin	0.72	1.6	6.00%	94.00%	0.00%	2.21
FPA-4	Margin	0.72	1.6	13.00%	87.00%	0.00%	1.56
FPA-5	Margin	0.72	1.6	3.00%	97.00%	0.00%	1.57

Table 2: Sample ID, abundance of each faunal grain type observed in Raivavae sediment samples. BR = bryozoan, CR = coral, CA = coralline algae, HA = *Halimeda*, MO = mollusk, EC = echinoderm, FR = foram, SP = spicule, SR = serpulid, CR = crustacean, & UN = unknown.

Raivavae												
Sample	BR	CR	CA	CA	HA	MO	EC	FR	SP	SR	CR	UN
FPA-8	0.00%	40.00%	17.00%	57.00%	18.00%	14.00%	0.00%	0.00%	0.00%	0.00%	0.00%	12.00%
FPA-17	0.00%	23.00%	22.00%	45.00%	28.00%	12.00%	1.00%	5.00%	0.00%	0.00%	0.00%	9.00%
FPA-16	0.00%	23.00%	19.00%	42.00%	38.00%	15.00%	0.00%	0.00%	0.00%	0.00%	0.00%	5.00%
FPA-11	1.00%	25.00%	21.00%	46.00%	28.00%	5.00%	0.00%	10.00%	0.00%	1.00%	0.00%	10.00%
FPA-20	0.00%	27.00%	16.00%	43.00%	19.00%	23.00%	0.00%	2.00%	0.00%	0.00%	0.00%	13.00%
FPA-26	0.00%	12.00%	0.00%	12.00%	63.00%	21.00%	0.00%	0.00%	0.00%	0.00%	0.00%	4.00%
FPA-22	1.00%	19.00%	11.00%	30.00%	42.00%	19.00%	0.00%	1.00%	0.00%	0.00%	0.00%	7.00%
FPA-19	0.00%	24.00%	1.00%	25.00%	56.00%	14.00%	0.00%	0.00%	0.00%	0.00%	0.00%	5.00%
FPA-6	0.00%	20.00%	8.00%	28.00%	69.00%	3.00%	0.00%	0.00%	0.00%	0.00%	0.00%	0.00%
FPA-28	0.00%	34.00%	6.00%	40.00%	16.00%	35.00%	0.00%	2.00%	1.00%	0.00%	0.00%	6.00%
FPA-13	0.00%	0.00%	0.00%	0.00%	71.00%	22.00%	0.00%	1.00%	0.00%	0.00%	0.00%	6.00%
FPA-29	2.00%	13.00%	3.00%	16.00%	51.00%	12.00%	0.00%	10.00%	0.00%	0.00%	0.00%	9.00%
FPA-2	0.00%	8.00%	0.00%	8.00%	58.00%	22.00%	1.00%	2.00%	0.00%	0.00%	0.00%	9.00%
FPA-10	1.00%	10.00%	0.00%	10.00%	56.00%	25.00%	0.00%	0.00%	0.00%	3.00%	0.00%	5.00%
FPA-9	0.00%	44.00%	4.00%	48.00%	19.00%	27.00%	2.00%	0.00%	1.00%	0.00%	0.00%	3.00%
FPA-24	0.00%	30.00%	14.00%	44.00%	33.00%	11.00%	6.00%	0.00%	1.00%	0.00%	0.00%	5.00%
FPA-25	0.00%	32.00%	9.00%	41.00%	31.00%	17.00%	1.00%	0.00%	2.00%	1.00%	0.00%	7.00%
FPA-1	1.00%	46.00%	27.00%	73.00%	15.00%	3.00%	2.00%	0.00%	0.00%	0.00%	0.00%	6.00%
FPA-18	0.00%	32.00%	10.00%	42.00%	26.00%	30.00%	1.00%	0.00%	1.00%	1.00%	0.00%	0.00%
FPA-21	0.00%	38.00%	4.00%	42.00%	22.00%	29.00%	0.00%	0.00%	0.00%	2.00%	0.00%	5.00%
FPA-12	0.00%	25.00%	15.00%	40.00%	26.00%	20.00%	5.00%	0.00%	2.00%	0.00%	0.00%	7.00%
FPA-30	0.00%	33.00%	19.00%	52.00%	12.00%	26.00%	0.00%	2.00%	0.00%	0.00%	0.00%	8.00%
FPA-15	0.00%	39.00%	6.00%	45.00%	22.00%	22.00%	2.00%	0.00%	6.00%	0.00%	0.00%	3.00%
FPA-14	0.00%	24.00%	11.00%	35.00%	45.00%	11.00%	4.00%	0.00%	0.00%	1.00%	0.00%	4.00%
FPA-23	0.00%	42.00%	8.00%	50.00%	16.00%	23.00%	0.00%	1.00%	0.00%	1.00%	0.00%	10.00%
FPA-3	0.00%	17.00%	11.00%	28.00%	27.00%	30.00%	0.00%	0.00%	1.00%	0.00%	0.00%	14.00%
FPA-4	0.00%	43.00%	3.00%	46.00%	18.00%	32.00%	0.00%	0.00%	0.00%	0.00%	0.00%	4.00%
FPA-5	0.00%	39.00%	14.00%	53.00%	16.00%	21.00%	3.00%	0.00%	1.00%	0.00%	0.00%	6.00%

Table 3: Sample ID, location, in terms of (Margin or Interior), RDRR, water depth, percent gravel, percent sand, percent mud, and sorting values of each of the sediment samples collected from the platform top of Tubuai.

Tubuai							
Sample	Location	RDRR	Depth (m)	Gravel	Sand	Mud	Sorting
FPA-70	Interior	0.45	21.76	5.00%	60.00%	35.00%	1.4
FPA-45	Interior	0.57	5.75	18.00%	82.00%	0.00%	1.32
FPA-57	Interior	0.59	15.94	5.00%	77.00%	18.00%	1.23
FPA-58	Interior	0.65	4.28	4.00%	96.00%	0.00%	0.85
FPA-55	Interior	0.77	1.64	28.00%	70.00%	2.00%	1.48
FPA-56	Interior	0.78	7.28	12.00%	85.00%	3.00%	1.59
FPA-60	Margin	0.09	5.31	17.00%	83.00%	0.00%	0.86
FPA-61	Margin	0.09	5.31	6.00%	94.00%	0.00%	0.87
FPA-59	Margin	0.12	12.11	10.00%	89.00%	0.00%	1.23
FPA-71	Margin	0.16	1.62	23.00%	75.00%	1.00%	1.38
FPA-69	Margin	0.2	0.74	63.00%	38.00%	0.00%	1.15
FPA-68	Margin	0.22	1.38	36.00%	64.00%	0.00%	1.2
FPA-54	Margin	0.47	1.8	36.00%	64.00%	0.00%	1.51
FPA-49	Margin	0.49	1.35	27.00%	72.00%	0.00%	0.91
FPA-53	Margin	0.6	1.37	18.00%	82.00%	0.00%	1.19
FPA-46	Margin	0.64	5.58	18.00%	82.00%	0.00%	1.05
FPA-48	Margin	0.64	1.89	18.00%	81.00%	0.00%	1.4
FPA-47	Margin	0.78	5.01	20.00%	79.00%	0.00%	1.52
FPA-50	Margin	0.81	3.29	23.00%	77.00%	0.00%	1.16
FPA-52	Margin	0.81	1.42	8.00%	92.00%	0.00%	1.05
FPA-51	Margin	0.86	2.69	30.00%	69.00%	0.00%	1.09

Table 4: Sample ID, abundance of each faunal grain type observed in Tubuai sediment samples. BR = bryozoan, CR = coral, CA = coralline algae, HA = *Halimeda*, MO = mollusk, EC = echinoderm, FR = foram, SP = spicule, SR = serpulid, CR = crustacean, & UN = unknown.

Tubuai												
Sample	BR	CR	CA	CA	HA	MO	EC	FR	SP	SR	CR	UN
FPA-70	0.00%	21.00%	9.00%	30.00%	35.00%	27.00%	0.00%	0.00%	0.00%	0.00%	0.00%	8.00%
FPA-45	0.00%	36.00%	13.00%	49.00%	13.00%	26.00%	0.00%	0.00%	3.00%	0.00%	0.00%	9.00%
FPA-57	0.00%	20.00%	18.00%	38.00%	25.00%	25.00%	0.00%	0.00%	0.00%	0.00%	0.00%	12.00%
FPA-58	0.00%	20.00%	15.00%	35.00%	25.00%	26.00%	2.00%	1.00%	3.00%	1.00%	0.00%	7.00%
FPA-55	0.00%	8.00%	5.00%	13.00%	59.00%	20.00%	0.00%	4.00%	0.00%	0.00%	0.00%	4.00%
FPA-56	0.00%	20.00%	14.00%	34.00%	41.00%	16.00%	1.00%	3.00%	0.00%	0.00%	0.00%	5.00%
FPA-60	0.00%	23.00%	13.00%	36.00%	26.00%	24.00%	5.00%	2.00%	1.00%	0.00%	0.00%	6.00%
FPA-61	0.00%	30.00%	5.00%	35.00%	32.00%	22.00%	3.00%	2.00%	0.00%	0.00%	1.00%	4.00%
FPA-59	0.00%	23.00%	14.00%	37.00%	23.00%	20.00%	6.00%	1.00%	1.00%	0.00%	2.00%	10.00%
FPA-71	0.00%	20.00%	14.00%	34.00%	20.00%	32.00%	6.00%	0.00%	0.00%	0.00%	0.00%	8.00%
FPA-69	0.00%	14.00%	7.00%	21.00%	42.00%	24.00%	11.00%	0.00%	0.00%	0.00%	0.00%	2.00%
FPA-68	0.00%	12.00%	14.00%	26.00%	34.00%	22.00%	6.00%	0.00%	2.00%	0.00%	0.00%	10.00%
FPA-54	0.00%	25.00%	11.00%	36.00%	19.00%	35.00%	2.00%	0.00%	1.00%	0.00%	0.00%	7.00%
FPA-49	0.00%	35.00%	8.00%	43.00%	22.00%	25.00%	1.00%	0.00%	1.00%	0.00%	0.00%	8.00%
FPA-53	0.00%	17.00%	11.00%	28.00%	23.00%	40.00%	3.00%	0.00%	0.00%	0.00%	0.00%	6.00%
FPA-46	0.00%	37.00%	10.00%	47.00%	15.00%	29.00%	2.00%	0.00%	0.00%	0.00%	0.00%	7.00%
FPA-48	0.00%	35.00%	17.00%	52.00%	15.00%	15.00%	2.00%	0.00%	3.00%	1.00%	0.00%	12.00%
FPA-47	0.00%	25.00%	15.00%	39.00%	33.00%	18.00%	2.00%	1.00%	0.00%	2.00%	0.00%	6.00%
FPA-50	0.00%	27.00%	9.00%	36.00%	27.00%	27.00%	4.00%	0.00%	2.00%	1.00%	0.00%	3.00%
FPA-52	0.00%	21.00%	10.00%	31.00%	18.00%	37.00%	3.00%	0.00%	2.00%	0.00%	0.00%	9.00%
FPA-51	0.00%	25.00%	8.00%	33.00%	23.00%	35.00%	2.00%	0.00%	1.00%	0.00%	0.00%	6.00%

Table 5: Location, in terms of (margin or interior), RDRR, water depth, percent coral (CR), and percent *Halimeda* (HA) of each of the sediment samples from the platform top of Bora Bora. Sample ID, water depth, CR, and HA from (Gischler (2011)).

Bora Bora					
Sample	Location	RDRR	Depth (m)	CR	HA
BB-10	Interior	0.91	9	53.00%	4.60%
BB-14	Interior	0.54	24	25.50%	6.10%
BB-15	Interior	0.65	22	8.40%	10.70%
BB-16	Interior	0.82	24	1.40%	2.10%
BB-18	Interior	0.28	13	48.30%	7.90%
BB-19	Interior	0.35	22	18.70%	9.10%
BB-20	Interior	0.49	26	6.00%	1.50%
BB-21	Interior	0.49	28	0.10%	0.20%
BB-22	Interior	0.79	26	0.00%	0.00%
BB-23	Interior	0.83	22	0.00%	0.20%
BB-24	Interior	0.88	20	5.80%	4.20%
BB-25	Interior	0.96	16	10.70%	7.90%
BB-28	Interior	0.62	18	8.50%	9.60%
BB-30	Interior	0.74	30	0.10%	0.30%
BB-5	Interior	0.61	35	0.40%	1.70%
BB-6	Interior	0.65	37	0.60%	0.40%
BB-7	Interior	0.72	34	0.20%	0.50%
BB-8	Interior	0.78	30	6.70%	9.00%
BB-9	Interior	0.83	29	11.20%	31.90%
BB-1	Margin	0.22	0.5	2.00%	4.80%
BB-11	Margin	0.56	3	31.80%	23.30%
BB-12	Margin	0.61	2	28.50%	39.00%
BB-13	Margin	0.38	2	40.70%	24.20%
BB-17	Margin	0.23	3	32.30%	14.90%
BB-2	Margin	0.51	5	2.80%	12.00%
BB-26	Margin	0.45	0.5	28.20%	40.50%
BB-29	Margin	0.45	4	8.40%	6.30%
BB-3	Margin	0.73	11	3.70%	1.60%
BB-31	Margin	0.07	0	50.70%	10.20%
BB-4	Margin	0.07	25	28.80%	21.20%

Table 6: Results from all 22 Raivavae water depth models as applied to each of the three subgroups of samples. RMSE is given in meters. NRMSE is the RMSE normalized to the depth ranges of the respective subgroup. NRMSE gives the error (on a scale of 0 – 1) of the model. Model structure represents the variables that were included in each model (1 = randomness model, MU = mud, SA = sand, GR = gravel, SO = sorting, CR = coral, and HA = *Halimeda*).

Water Depth (m)							
Model #	Model Structure	RMSE (Platform-wide)	NRMSE (Platform-wide)	RMSE (Margin)	NRMSE (Margin)	RMSE (Interior)	NRMSE (Interior)
0	1	3.37	0.2378	0.83	0.2277	2.93	0.2576
1	MU	3.34	0.2358	0.80	0.2197	2.92	0.2572
2	SA	3.31	0.2340	0.80	0.2194	2.93	0.2576
3	GR	3.16	0.2233	0.83	0.2271	2.93	0.2576
4	SO	3.21	0.2269	0.76	0.2075	2.92	0.2569
5	CR	2.74	0.1934	0.72	0.1975	2.69	0.2372
6	HA	2.83	0.2000	0.73	0.2013	2.81	0.2476
7	MU + SA	3.14	0.2220	0.80	0.2192	2.92	0.2571
8	MU + GR	3.15	0.2224	0.80	0.2197	2.92	0.2572
9	MU + SO	3.11	0.2195	0.75	0.2054	2.90	0.2552
10	MU + CR	2.69	0.1896	0.69	0.1895	2.65	0.2332
11	MU + HA	2.71	0.1914	0.73	0.1999	2.77	0.2436
12	SA + GR	3.15	0.2226	0.80	0.2193	2.93	0.2576
13	SA + SO	3.21	0.2268	0.75	0.2058	2.91	0.2565
14	SA + CR	2.73	0.1928	0.69	0.1900	2.69	0.2372
15	SA + HA	2.83	0.1996	0.73	0.1997	2.80	0.2462
16	GR + SO	3.09	0.2185	0.73	0.1987	2.92	0.2569
17	GR + CR	2.62	0.1850	0.72	0.1962	2.69	0.2365
18	GR + HA	2.77	0.1956	0.73	0.1998	2.81	0.2475
19	SO + CR	2.70	0.1907	0.69	0.1902	2.62	0.2303
20	SO + HA	2.78	0.1965	0.69	0.1883	2.80	0.2464
21	CR + HA	2.72	0.1921	0.70	0.1931	2.68	0.2362

Table 7: Results from all 22 Tubuai water depth models as applied to each of the three subgroups of samples. NRMSE is the RMSE normalized to the depth ranges of the respective subgroup. NRMSE gives the error (on a scale of 0 – 1) of the model. Model structure represents the variables that were included in each model (1 = randomness model, MU = mud, SA = sand, GR = gravel, SO = sorting, CR = coral, and HA = *Halimeda*).

Water Depth (m)							
Model #	Model Structure	RMSE (Platform-wide)	NRMSE (Platform-wide)	RMSE (Margin)	NRMSE (Margin)	RMSE (Interior)	NRMSE (Interior)
0	1	5.25	0.2498	2.86	0.2513	7.07	0.3513
1	MU	4.36	0.2075	2.48	0.2178	5.41	0.2689
2	SA	5.25	0.2496	2.48	0.2178	5.67	0.2816
3	GR	2.68	0.1277	2.82	0.2478	1.98	0.0983
4	SO	5.19	0.2468	2.84	0.2502	7.03	0.3496
5	CR	5.25	0.2498	2.79	0.2452	7.00	0.3481
6	HA	5.24	0.2494	2.85	0.2510	6.90	0.3432
7	MU + SA	2.28	0.1085	2.48	0.2178	1.48	0.0734
8	MU + GR	2.27	0.1082	2.43	0.2135	1.48	0.0734
9	MU + SO	4.20	0.1996	2.48	0.2178	4.05	0.2013
10	MU + CR	4.31	0.2053	2.48	0.2178	5.41	0.2688
11	MU + HA	4.23	0.2010	2.38	0.2089	5.31	0.2638
12	SA + GR	2.28	0.1083	2.44	0.2143	1.48	0.0734
13	SA + SO	5.17	0.2458	2.48	0.2177	5.27	0.2620
14	SA + CR	5.25	0.2496	2.48	0.2178	5.26	0.2616
15	SA + HA	5.23	0.2489	2.38	0.2096	4.43	0.2200
16	GR + SO	2.67	0.1272	2.81	0.2475	1.95	0.0968
17	GR + CR	2.57	0.1220	2.76	0.2430	1.43	0.0711
18	GR + HA	2.63	0.1250	2.81	0.2470	1.26	0.0624
19	SO + CR	5.18	0.2465	2.78	0.2448	6.95	0.3454
20	SO + HA	5.19	0.2468	2.84	0.2497	6.67	0.3315
21	CR + HA	5.23	0.2486	2.78	0.2442	6.85	0.3407

Table 8: Results from all 4 Bora Bora water depth models as applied to each of the three subgroups of samples. RMSE is given in meters. NRMSE is the RMSE normalized to the depth ranges of the respective subgroup. NRMSE gives the error (on a scale of 0 – 1) of the model. Model structure represents the variables that were included in each model (1 = randomness model, CR = coral, and HA = *Halimeda*).

Water Depth (m)							
Model #	Model Structure	RMSE (Platform-wide)	NRMSE (Platform-wide)	RMSE (Margin)	NRMSE (Margin)	RMSE (Interior)	NRMSE (Interior)
0	1	11.73	0.3170	6.93	0.2772	7.18	0.2566
1	CR	9.58	0.2588	6.87	0.2748	4.93	0.1760
2	HA	10.25	0.2771	6.88	0.2753	7.11	0.2541
3	CR + HA	9.14	0.2471	6.86	0.2743	4.92	0.1758

Table 9: Results from all 22 Raivavae RDRR models as applied to each of the three subgroups of samples. RMSE is given in meters. NRMSE is the RMSE normalized to the ranges of RDRR measurements of the respective subgroup. The model structure represents the variables that were included in each model (1 = randomness model, MU = mud, SA = sand, GR = gravel, SO = sorting, CR = coral, and HA = *Halimeda*).

RDRR							
Model #	Model Structure	RMSE (Platform-wide)	NRMSE (Platform-wide)	RMSE (Margin)	NRMSE (Margin)	RMSE (Interior)	NRMSE (Interior)
0	1	0.2044	0.2839	0.1884	0.3426	0.1916	0.3091
1	MU	0.1958	0.2720	0.1552	0.2823	0.1903	0.3069
2	SA	0.2037	0.2829	0.1541	0.2802	0.1911	0.3083
3	GR	0.2023	0.2809	0.1884	0.3425	0.1916	0.3090
4	SO	0.2044	0.2839	0.1739	0.3162	0.1911	0.3082
5	CR	0.1727	0.2399	0.1858	0.3379	0.1495	0.2411
6	HA	0.1798	0.2497	0.1869	0.3397	0.1545	0.2491
7	MU + SA	0.1942	0.2698	0.1536	0.2793	0.1902	0.3068
8	MU + GR	0.1946	0.2703	0.1515	0.2754	0.1903	0.3069
9	MU + SO	0.1947	0.2704	0.1506	0.2738	0.1903	0.3069
10	MU + CR	0.1602	0.2225	0.1511	0.2748	0.1492	0.2407
11	MU + HA	0.1610	0.2236	0.1546	0.2810	0.1531	0.2469
12	SA + GR	0.1956	0.2716	0.1521	0.2765	0.1887	0.3043
13	SA + SO	0.2033	0.2824	0.1506	0.2738	0.1910	0.3080
14	SA + CR	0.1680	0.2333	0.1493	0.2714	0.1491	0.2405
15	SA + HA	0.1680	0.2333	0.1534	0.2790	0.1522	0.2455
16	GR + SO	0.2020	0.2806	0.1714	0.3116	0.1908	0.3078
17	GR + CR	0.1725	0.2396	0.1858	0.3378	0.1489	0.2402
18	GR + HA	0.1798	0.2497	0.1865	0.3390	0.1532	0.2471
19	SO + CR	0.1695	0.2354	0.1611	0.2929	0.1376	0.2219
20	SO + HA	0.1777	0.2468	0.1737	0.3159	0.1530	0.2467
21	CR + HA	0.1725	0.2395	0.1758	0.3197	0.1473	0.2376

Table 10: Results from all 22 Tubuai RDRR models as applied to each of the three subgroups of samples. RMSE is given in meters. NRMSE is the RMSE normalized to the ranges of RDRR measurements of the respective subgroup. The model structure represents the variables that were included in each model (1 = randomness model, MU = mud, SA = sand, GR = gravel, SO = sorting, CR = coral, and HA = *Halimeda*).

RDRR							
Model #	Model Structure	RMSE (Platform-wide)	NRMSE (Platform-wide)	RMSE (Margin)	NRMSE (Margin)	RMSE (Interior)	NRMSE (Interior)
0	1	0.2582	0.3353	0.2825	0.3669	0.1154	0.3497
1	MU	0.2551	0.3313	0.2808	0.3647	0.0971	0.2942
2	SA	0.2550	0.3312	0.2809	0.3648	0.1047	0.3173
3	GR	0.2582	0.3353	0.2704	0.3512	0.0782	0.2370
4	SO	0.2480	0.3221	0.2754	0.3577	0.1114	0.3376
5	CR	0.2571	0.3339	0.2683	0.3484	0.0996	0.3018
6	HA	0.2582	0.3353	0.2632	0.3418	0.0941	0.2852
7	MU + SA	0.2547	0.3308	0.2806	0.3644	0.0748	0.2267
8	MU + GR	0.2546	0.3306	0.2686	0.3488	0.0748	0.2267
9	MU + SO	0.2429	0.3155	0.2718	0.3530	0.0970	0.2939
10	MU + CR	0.2546	0.3306	0.2682	0.3483	0.0863	0.2615
11	MU + HA	0.2547	0.3308	0.2619	0.3401	0.0885	0.2682
12	SA + GR	0.2547	0.3308	0.2689	0.3492	0.0748	0.2267
13	SA + SO	0.2396	0.3112	0.2716	0.3527	0.0772	0.2339
14	SA + CR	0.2547	0.3308	0.2682	0.3483	0.0751	0.2276
15	SA + HA	0.2543	0.3303	0.2620	0.3403	0.0445	0.1348
16	GR + SO	0.2474	0.3213	0.2556	0.3319	0.0648	0.1964
17	GR + CR	0.2570	0.3338	0.2597	0.3373	0.0458	0.1388
18	GR + HA	0.2582	0.3353	0.2431	0.3157	0.0404	0.1224
19	SO + CR	0.2446	0.3177	0.2566	0.3332	0.0973	0.2948
20	SO + HA	0.2473	0.3212	0.2579	0.3349	0.0939	0.2845
21	CR + HA	0.2556	0.3319	0.2605	0.3383	0.0941	0.2852

Table 11: Results from all 4 Bora Bora water RDRR as applied to each of the three subgroups of samples. RMSE is given in meters. NRMSE is the RMSE normalized to the ranges of RDRR measurements of the respective subgroup. The model structure represents the variables that were included in each model (1 = randomness model, CR = coral, and HA = *Halimeda*).

RDRR							
Model #	Model Structure	RMSE (Platform-wide)	NRMSE (Platform-wide)	RMSE (Margin)	NRMSE (Margin)	RMSE (Interior)	NRMSE (Interior)
0	1	0.2382	0.2676	0.2076	0.3145	0.1827	0.2687
1	CR	0.2125	0.2388	0.1872	0.2836	0.1777	0.2613
2	HA	0.2311	0.2597	0.2055	0.3113	0.1823	0.2681
3	CR + HA	0.2123	0.2386	0.1679	0.2543	0.1762	0.2591